Atmos. Chem. Phys., 11, 8827–8845, 2011
www.atmos-chem-phys.net/11/8827/2011/
doi:10.5194/acp-11-8827-2011

Atmospheric Chemistry and Physics

Elemental composition and oxidation of chamber organic aerosol

P. S. Chhabra[1], N. L. Ng[2], M. R. Canagaratna[2], A. L. Corrigan[3], L. M. Russell[3], D. R. Worsnop[2], R. C. Flagan[1,4], and J. H. Seinfeld[1,4]

[1]Division of Chemistry and Chemical Engineering, California Institute of Technology, Pasadena, CA, USA
[2]Aerodyne Research, Inc. Billerica, MA, USA
[3]Scripps Institution of Oceanography, University of California, San Diego, CA, USA
[4]Division of Engineering and Applied Science, California Institute of Technology, Pasadena, CA, USA

Received: 21 March 2011 – Published in Atmos. Chem. Phys. Discuss.: 30 March 2011
Revised: 15 August 2011 – Accepted: 24 August 2011 – Published: 1 September 2011

Abstract. Recently, graphical representations of aerosol mass spectrometer (AMS) spectra and elemental composition have been developed to explain the oxidative and aging processes of secondary organic aerosol (SOA). It has been shown previously that oxygenated organic aerosol (OOA) components from ambient and laboratory data fall within a triangular region in the f_{44} vs. f_{43} space, where f_{44} and f_{43} are the ratios of the organic signal at *m/z* 44 and 43 to the total organic signal in AMS spectra, respectively; we refer to this graphical representation as the "triangle plot." Alternatively, the Van Krevelen diagram has been used to describe the evolution of functional groups in SOA. In this study we investigate the variability of SOA formed in chamber experiments from twelve different precursors in both "triangle plot" and Van Krevelen domains. Spectral and elemental data from the high-resolution Aerodyne aerosol mass spectrometer are compared to offline species identification analysis and FTIR filter analysis to better understand the changes in functional and elemental composition inherent in SOA formation and aging. We find that SOA formed under high- and low-NO_x conditions occupy similar areas in the "triangle plot" and Van Krevelen diagram and that SOA generated from already oxidized precursors allows for the exploration of areas higher on the "triangle plot" not easily accessible with non-oxidized precursors. As SOA ages, it migrates toward the top of the triangle along a path largely dependent on the precursor identity, which suggests increasing organic acid content and decreasing mass spectral variability. The most oxidized SOA come from the photooxidation of methoxyphenol precursors which yielded SOA O/C ratios near unity. α-pinene ozonolysis and naphthalene photooxidation SOA systems have had the highest degree of mass closure in previous chemical characterization studies and also show the best agreement between AMS elemental composition measurements and elemental composition of identified species within the uncertainty of the AMS elemental analysis. In general, compared to their respective unsaturated SOA precursors, the elemental composition of chamber SOA follows a slope shallower than -1 on the Van Krevelen diagram, which is indicative of oxidation of the precursor without substantial losss of hydrogen, likely due to the unsaturated nature of the precursors. From the spectra of SOA studied here, we are able to reproduce the triangular region originally constructed with ambient OOA compents with chamber aerosol showing that SOA becomes more chemically similar as it ages. Ambient data in the middle of the triangle represent the ensemble average of many different SOA precursors, ages, and oxidative processes.

1 Introduction

Organic compounds comprise a significant fraction of ambient submicron aerosol mass (Zhang et al., 2007; Jimenez et al., 2009) with numerous sources and atmospheric processes contributing to their chemical complexity (Hallquist et al., 2009). Secondary organic aerosol (SOA) forms from the gas-phase oxidation of a number of anthropogenic and biogenic volatile organic compounds (VOCs) (Kroll and Seinfeld, 2008; Robinson et al., 2007; Lim et al., 2010; Donahue et al., 2009; Goldstein and Galbally, 2007; De Gouw and Jimenez, 2009). Although typically only a portion of the multitude of compounds present in SOA can be identified on a molecular level, on-line instruments like the Aerodyne Aerosol Mass Spectrometer (AMS) (Jayne et al., 2000; Canagaratna et al., 2007) can provide bulk, chemical characterization in real-time.

Correspondence to: J. H. Seinfeld
(seinfeld@caltech.edu)

Published by Copernicus Publications on behalf of the European Geosciences Union.

Recently, two important methods using AMS data to characterize the chemical nature of OA have been proposed. Heald et al. (2010) applied the Van Krevelen diagram to the bulk elemental composition of ambient and laboratory OA formed under a wide range of reaction conditions. Previous investigations have used the Van Krevelen diagram to map individual masses identified by high resolution electrospray ionization mass spectrometry (ESI-MS), but not for OA as a whole (Reinhardt et al., 2007; Walser et al., 2008; Bateman et al., 2009). Originally developed to describe the elemental composition of coal, the Van Krevelen diagram has axes of hydrogen to carbon (H/C) molar ratios and oxygen to carbon (O/C) molar ratios. Changes in functionality of OA are traced in this space along a line of a particular slope. For instance, when an aliphatic functionality is replaced by a carbonyl functionality, the resulting line on a Van Krevelen has a slope of -2. Substituting aliphatic to alcohol or peroxide functionality produces a line with a slope of zero. Addition of carboxylic acids or hydroxycarbonyls gives a -1 slope. Hydration or condensation reactions follow a line with a slope of +2. Heald et al. (2010) found that bulk OA elemental ratios from both laboratory and ambient atmospheres occupy a tight range on the Van Krevelen diagram with a slope of -1, implying that OA aging involves, on average, the addition of carboxylic acids or equal amounts of alcohol and carbonyl functionalities.

Ng et al. (2010) used positive matrix factorization techniques (Zhang et al., 2005; Lanz et al., 2007; Ulbrich et al., 2009) and compiled the factor analysis for 43 Northern Hemisphere AMS datasets of OA. They found that at most sites AMS spectra can be separated into oxygenated OA (OOA) and hydrocarbon-like OA (HOA) components (Zhang et al., 2007). For many datasets, OOA was further subcategorized into low-volatility OOA (LV-OOA) and semi-volatile OOA (SV-OOA) (Jimenez et al., 2009). LV-OOA has been described as aged OOA, with spectra dominated by mass fragment CO_2^+ at *m/z* 44, and SV-OOA, described as "fresh" OOA with an intense signal at $C_2H_3O^+$ at *m/z* 43 as well. Mass fragment CO_2^+ has been considered a marker ion for organic acids in OA, as it is known to form from the thermal decarboxylation of many different oxo-, di-, and polycarboxylic acids (Alfarra, 2004; Aiken et al., 2007; Takegawa et al., 2007; Duplissy et al., 2011). Fragment ion $C_2H_3O^+$, conversely, has been hypothesized to form from non-acid oxygen-containing organic compounds. Since *m/z* 43 and 44 are the dominant ions in SV- and LV-OOA spectra and represent different functionalities, Ng et al. (2010) plotted f_{44} vs. f_{43} for all OOA spectra from different sites, where f_{44} and f_{43} are the ratios of *m/z* 44 and *m/z* 43 to the total OA signal in the spectrum, respectively. Ng et al. (2010) found that the OOA components clustered into a triangular region with wide variability across f_{43} at low values of f_{44} that narrows as f_{44} increases. As a consequence, LV-OOA data tend to group in the top half of the "triangle plot" and SV-OOA in the lower half. Ng et al. (2010) concluded that OOA components become more similar in terms of oxidation state with increasing photochemical age, regardless of source. The most oxidized spectra tend to resemble that of fulvic acid.

Chamber experiments have long been the gold standard to determine SOA formation mechanisms and to constrain the chemistry and yields of SOA. Chamber studies, however, cannot typically reach the oxidant exposures achieved in the ambient atmosphere (Rudich et al., 2007; Kroll and Seinfeld, 2008; Hallquist et al., 2009). Most recently in the context of AMS spectral factors, the studies of both Chhabra et al. (2010) and Ng et al. (2010) found that SOA from chamber studies typically does not reach the degree of oxygenation of ambient LV-OOA. For example, Heald et al. (2010) presented data from Shilling et al. (2009), in which the most oxidized SOA from α-pinene ozonolysis has an O/C of approximately 0.4, whereas SOA from the MILAGRO (Mexico City) campaign (Aiken et al., 2009) surpasses 0.6. Ng et al. (2010) noted that most laboratory chamber data fall into the lower half of the "triangle plot", showing that laboratory OA is closer to SV-OOA than LV-OOA. Like SV-OOA, chamber SOA has high variability in f_{43}, likely a result of the variety of precursors, oxidants, and other experimental variables. In chamber investigations in which SOA is generated at total organic loadings higher than those of ambient OA, more volatile, less oxygenated species partition into the particle phase than would at lower aerosol loadings. Additionally, chamber experiments are typically carried out for less than $\sim$ 24 h, shorter than the atmospheric lifetime ($\sim$1 week) of ambient aerosol, and therefore not accessing further oxidation that might be occurring over this extended time scale. A comprehensive study by Chhabra et al. (2010) compared the elemental composition of five different chamber systems and found that monoaromatic- and naphthalene-derived SOA can reach O/C ratios upward of 0.7, approaching those of ambient measurements, and thus emphasizing the importance of OH exposure and precursor identity on SOA oxidation state.

In this study, we build on the previous investigation of Chhabra et al. (2010) by exploring the variability of chamber SOA in both Van Krevelen and "triangle plot" spaces. In addition to the systems studied in Chhabra et al. (2010) (glyoxal uptake, α-pinene ozonolysis, isoprene photooxidation, monoaromatic photooxidation, and naphthalene photooxidation), we present high-resolution time-of-flight AMS (HR-ToF-AMS) spectra and elemental composition of chamber SOA from α-pinene photooxidation, methoxyphenol photooxidation, and unsaturated aldehyde photooxidation. Structures for each of the twelve precursors are shown in Figure 1. We compare the elemental composition as measured by the AMS to molecular species identified by off-line methods for each SOA system as well as FTIR measurements of α-pinene photooxidation and guaiacol photooxidation SOA. The goal of this work is to assess the extent to which SOA molecular and functional group composition analyses support the overall analysis of SOA formation and aging as represented in the Van Krevelen and "triangle plot" spaces.

2 Experimental section

2.1 Chamber operation

Chamber operation and experimental methods for glyoxal uptake, α-pinene ozonolysis, monoaromatic, isoprene, and naphthalene photooxidation experiments are described in Chhabra et al. (2010). Experimental methods for α-pinene, methoxyphenol, and aldehyde photooxidation were nearly identical and are described in detail in Chan et al. (2010). In experiments in which methyl nitrite (CH_3ONO) was used as the OH precursor, CH_3ONO was vaporized into an evacuated 500 mL glass bulb and introduced into the chamber with an air stream of 5 L min^{-1}. The mixing ratio of CH_3ONO injected was estimated to be 200-400 ppb, based on the vapor pressure in the glass bulb measured using a capacitance manometer (MKS). Experimental conditions for each system are summarized in Table 1. All experiments were performed in the Caltech dual 28 m^3 Teflon laboratory chambers (Cocker et al., 2001; Keywood et al., 2004) over the period 2007–2010. Each chamber has a dedicated Differential Mobility Analyzer (DMA, TSI model 3081) coupled with a condensation nucleus counter (TSI model 3760) for measuring aerosol size distribution and number and volume concentration. Temperature, relative humidity (RH), ozone (O_3), NO, and NO_x were continuously monitored. For seeded experiments, ammonium sulfate seed particles were generated by atomization of a dilute aqueous ammonium sulfate solution using a constant rate atomizer.

2.2 High-Resolution Time-of-Flight Aerosol Mass Spectrometer

HR-ToF-AMS (Canagaratna et al., 2007; DeCarlo et al., 2006) spectra were analyzed as described in Chhabra et al. (2010). Briefly, in the mode of operation, the AMS was switched once every minute between the high-resolution "W-mode" and the lower resolution, higher sensitivity "V-mode". The "V-mode" data were analyzed using a fragmentation table to separate sulfate, ammonium, and organic spectra and to time-trace specific mass-to-charge ratios (Allan et al., 2004). "W-mode" data were analyzed using a separate high-resolution spectra toolbox known as PIKA to determine the chemical formulas contributing to distinct mass-to-charge (*m/z*) ratios (DeCarlo et al., 2006). "V-mode" data were used in "triangle plots" and "W-mode" data were used in Van Krevelen diagrams.

Default values were used for the CO_2^+ signal originating from chamber air as FTIR measurements showed the concentration of CO_2 in the chamber air is nominally the same as that in the atmosphere. Ratios of the particle-phase signals of CO^+ to CO_2^+ were determined to be close to 1 (Supplement) for most experiments so this value was used for all experiments except those of glyoxal uptake for which a value of 5 was used. The signals from H_2O^+, OH^+, and O^+ in the particulate organic mass may suffer interference from gas-phase H_2O, and their organic contributions were estimated as suggested in Aiken et al. (2008). Particulate nitrogen signals were observed in high-NO_x photooxidation experiments, originating mostly from NO^+ and NO_2^+ ions. Although gas-phase nitric acid is produced from the $OH + NO_2$ reaction, at low chamber humidities nitric acid is not expected to partition appreciably into the particle phase. Thus, the signals of NO^+ and NO_2^+ ions were included as part of the organic mass in high-NO_x photooxidation experiments.

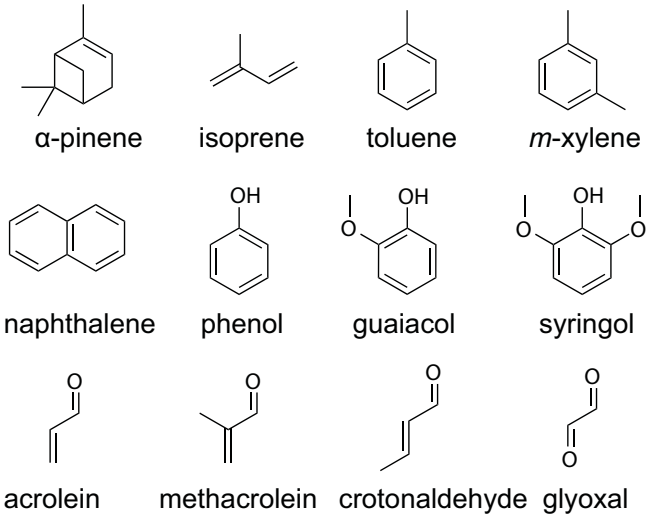

Fig. 1. Structures of the SOA precursors presented in this study.

2.3 Fourier Transform Infrared Spectroscopy (FTIR)

Samples for FTIR analysis were collected on Teflon filters (Pall Inc., Ann Arbor, MI, 37 mm diameter, 1.0 µm pore size, teflo membrane), following the collection, storage, analysis, and peak-fitting techniques described by Russell et al. (2009). Specifically, a Bruker Tensor 27 FTIR Spectrometer with a DTGS detector (Bruker, Waltham, MA) was used to scan filters before and after sample collection; samples were frozen during transport and storage to reduce evaporative loss of organics and reaction. An automated algorithm was used for subtracting Teflon (using the pre-scanned spectra) and ammonium, baselining, peak-fitting, and error estimation (Russell et al., 2009). Mass concentrations of alkane, carboxylic acid, hydroxyl, amine, non-acid carbonyl, organonitrate, alkene, and aromatic functional groups were quantified using previously reported algorithms and standards (Russell et al., 2009; Day et al., 2010).

FTIR O/C and H/C ratios were determined from measured organic bond absorbances by calculating the estimated moles of oxygen, carbon, and hydrogen associated with each measured bond and its associated functional group, as described in the Supplement (Russell et al., 2009; Russell, 2003). Since

Table 1. Experimental conditions and results.

Expt.#	VOC System	Oxidant Precursor	RH (%)	$[NO]_0$ (ppb)	$[NO_2]_0$ (ppb)	VOC Reacted (ppb)	Seed Vol. ($\mu m^3\ cm^{-3}$)	ΔM_0(Max)[d] ($\mu g\ m^{-3}$)
1	glyoxal uptake	–	60	<det[a]	<det[a]	182[b]	87	68.3
2	α-pinene	O_3	5.4	<det[a]	<det[a]	50[c]	12.5	62.0
3	α-pinene + OH	H_2O_2	4.2	<det[a]	<det[a]	46	13.7	63.9
4	α-pinene + OH	CH_3ONO	4.9	447	400	47	15.4	53.7
5	isoprene + OH	H2O2	5.2	<det[a]	<det[a]	49	16.2	8.2
6	isoprene + OH	HONO	< 10	536	400	267	11.7	10.0
7	toluene + OH	H_2O_2	< 10	<det[a]	<det[a]	112	10.9	151.3
8	toluene + OH	HONO	< 10	583	423	136	9.3	54.3
9	*m*-xylene + OH	H_2O_2	< 10	<det[a]	<det[a]	114	9.8	200.9
10	*m*-xylene + OH	HONO	< 10	501	538	200	9.3	55.2
11	naphthalene + OH	H_2O_2	8.3	<det[a]	<det[a]	20[c]	10.5	70.9
12	naphthalene + OH	HONO	6.3	431	370	25[c]	12.8	43.8
13	phenol + OH	H_2O_2, nucleation	4.9	<det[a]	<det[a]	21	0.1	30.5
14	phenol + OH	HONO, nucleation	3.7	332	545	19	0.0	24.8
15	guaiacol + OH	H_2O_2	5.7	<det[a]	<det[a]	6	16.3	11.9
16	guaiacol + OH	HONO	4.8	267	427	7	12.6	12.8
17	syringol + OH	H_2O_2	3.7	<det[a]	<det[a]	108	10.8	228
18	syringol + OH	HONO, nucleation	3.7	<det[a]	<det[a]	50	0.0	34.8
19	acrolein + OH	HONO	7.2	215	389	412	13.2	21.3
20	methacrolein + OH	HONO	9.3	725	368	186	11.4	10.1
21	crotonaldehyde + OH	HONO	9.0	215	370	252	12.1	14.0

[a] Below the detection limit of the measurement.
[b] Equilibrium concentration.
[c] approximate initial concentration.
[d] Mass loadings are calculated by multiplying the change in DMA volume by an estimated density. Estimated densities of glyoxal, α-pinene, isoprene (and unsaturated aldehydes), monoaromatics, and naphthalene SOA were taken from Galloway et al. (2009); Bahreini et al. (2005); Kroll et al. (2006); Ng et al. (2007); Chan et al. (2009) respectively.

alkene groups were below detection, an upper bound was considered to be their detection limit and a lower bound was considered zero. The degree of saturation for other functional groups was weighted by the saturation in the reactants (α-pinene and guaiacol). Hydrogen associated with amine groups was omitted since it is assumed that any ammonium is part of the inorganic seed rather than SOA.

3 Results

Elemental composition and high resolution-spectra of SOA derived from α-pinene ozonolysis, glyoxal uptake into seed aerosol, and monoaromatic, isoprene, and naphthalene photooxidation have been described in detail in Chhabra et al. (2010). Tabulated elemental ratios and high-resolution spectra for α-pinene, methoxyphenol, and unsaturated aldehyde photooxidation SOA are provided in the Supplementary Material. High-resolution spectra for SOA formed under similar conditions for each parent organic were identical; thus, one experiment for each system is presented. Raw measurement of elemental ratios requires calibration factors derived from the elemental analysis of laboratory standards. The calibration factors determined by Aiken et al. (2008) of 0.91 for H/C and 0.75 for O/C were used. The uncertainty estimates of the calibration factors reported for O/C and H/C are 31 % and 10 % respectively. Uncertainty in AMS elemental analysis and offline speciation is discussed in detail in Chhabra et al. (2010).

3.1 α-pinene SOA

Figure 2 illustrates the "triangle plot" (Panel a) and Van Krevelen diagram (Panels b and c) for SOA derived from α-pinene ozonolysis and photooxidation. The time progression of each system is illustrated in Panel a with open and closed circles representing the beginning and end of each experiment, respectively. Consistent with previous studies (Chhabra et al., 2010; Shilling et al., 2009), as the SOA mass formed by α-pinene ozonolysis increases, the O/C ratio and f_{44} decrease, behavior that is a result of increased partitioning of less oxidized semivolatile compounds into a growing OA medium. Oxygen-to-carbon ratios for α-pinene photooxidation SOA are approximately the same as those of ozonolysis SOA, however H/C ratios are slightly higher at 1.6. Similar to α-pinene ozonolysis SOA, the O/C ratios of photooxidation SOA under both NO_x conditions decrease as OA mass increases, behavior manifested in the Van Krevelen

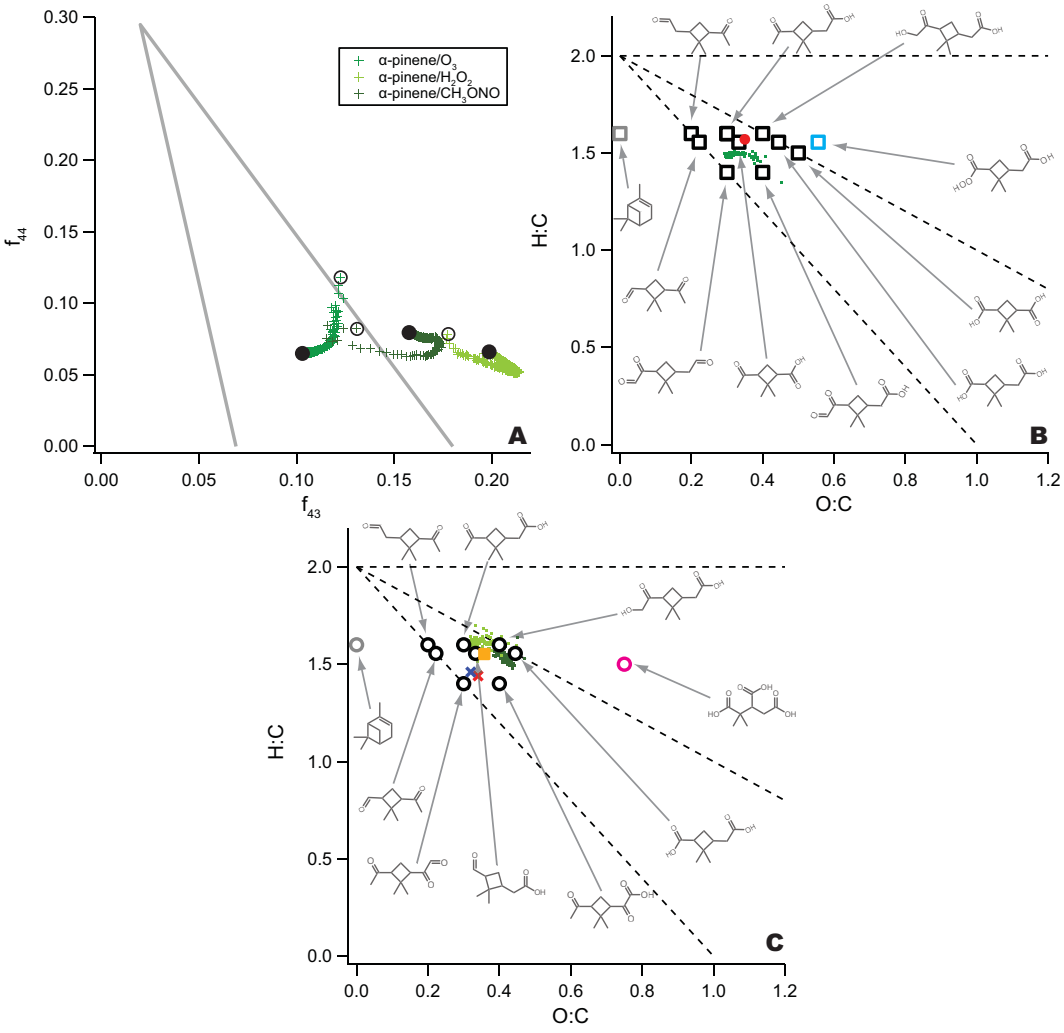

Fig. 2. **(A)** "Triangle plot" for α-pinene SOA formed from ozonolysis and high- and low-NO_x photooxidation. Here and in subsequent figures, the outline of the triangle (Ng et al., 2010) is shown in gray. Open and closed black circles represent the beginning and end of the experiments, respectively. **(B)** Van Krevelen diagram for SOA formed from α-pinene ozonolysis. α-pinene and SOA products identified by Yu et al. (1999) represented by gray and black boxes respectively. The molar weighted average of the elemental ratios of identified SOA products is represented by the red circle (Chhabra et al., 2010). The blue square denotes peroxypinic acid, a product of α-pinene ozonolysis proposed by Docherty et al. (2005). Here and in subsequent figures, lines with slopes of 0, −1 and −2 are represented by dashed lines. **(C)** Van Krevlen diagram for SOA formed from the high- and low-NO_x photooxidation of α-pinene. α-pinene and SOA products identified by Jaoui and Kamens (2001) and Szmigielski et al. (2007) are represented by black and pink circles, respectively. The mass weighted average O/C and H/C calculated from Jaoui and Kamens (2001) is represnted by an orange square. Elemental ratios as measured by FTIR data are represented by red (low-NO_x) and blue (high-NO_x) crosses.

diagram but more readily apparent in the "triangle plot" with decreases in f_{44} and increases in f_{43}. In contrast to ozonolysis SOA, however, photooxidation processes eventually overtake semivolatile partitioning and the oxidation state of photooxidation SOA increases, represented by increases in f_{44} (Ng et al., 2010). Towards the end of α-pinene photooxidation experiments, data in Panel a tend to migrate toward the top of the "triangle plot".

The elemental composition of identified compounds in α-pinene SOA are also shown on the Van Krevelen diagrams in Fig. 2 (Panels b and c). Chhabra et al. (2010) found close agreement between the bulk elemental ratios measured by the AMS and those of compounds detected by offline GC-MS by Yu et al. (1999), who were able to identify >90 % of the α-pinene ozonolysis SOA mass. The species identified by Yu et al. (1999) are represented in Panel b by black squares and closely agree with AMS data. Peroxypinic acid, represented by the blue square, is a product of α-pinene ozonolysis

proposed by Docherty et al. (2005) and is an approximate O/C upper bound. Similar elemental compositions to those measured by the AMS have also been measured by other methods (Tolocka et al., 2006; Reinhardt et al., 2007).

Many of the same products identified in α-pinene ozonolysis SOA have been identified in photooxidation SOA (Panel c) by Jaoui and Kamens (2001) (black circles), who determined that particle-phase products accounted for approximately 20 % of the reacted carbon. Using their particle-phase carbon yields, we calculate an average H/C and O/C ratio of 1.56 and 0.36 (represented by an orange square in Fig. 2, Panel c), closely agreeing with AMS measurements but slightly higher than those measured from FTIR analysis. Tri-carboxylic acid species (pink circle) observed in ambient aerosol filter samples have been proposed as photooxidation products of α-pinene (Szmigielski et al., 2007), though it is unlikely the α-pinene photooxidation experiments achieved OH exposures high enough to form these highly oxygenated species in substantial concentrations.

Since the publication of Yu et al. (1999) and Jaoui and Kamens (2001), several studies have identified oligoesters of α-pinene photooxidation and ozonolysis products in the particle phase (Gao et al., 2004; Müller et al., 2008; Hall and Johnston, 2011). Gao et al. (2004) and Hall and Johnston (2011) have estimated oligomers to account for 50 % of α-pinene SOA mass. It is possible that sample work up in speciation studies hydrates oligomers, separating them into the identified monomers and moving them up the Van Krevelen diagram along a line of slope 2. The original oligomers would reside further to the bottom left of the Van Krevelen diagram. As speciation of oligomers improves, the effect of oligomerization on the SOA elemental composition can be better constrained.

3.2 Isoprene SOA

The triangle and Van Krevelen plots for isoprene-photooxidation SOA appear in Fig. 3. The Van Krevelen diagram (Panel b) illustrates that the SOA elemental composition does not change appreciably over the course of the oxidation or at different NO_x concentrations (Chhabra et al., 2010). However, f_{44} increases as f_{43} decreases over the course of the experiment for both NO_x conditions (Panel a), suggesting that organic acid content increases with continued oxidation. High-NO_x spectra also display higher f_{44} values than low-NO_x spectra, consistent with filter measurements identifying methylglyceric acid oligomers as the dominant species in high-NO_x SOA and non-acid methyltetrols as the dominant species in low-NO_x SOA. Panel a shows that data for both systems migrate to the top of the triangle with continued photooxidation.

The main species and classes of compounds identified in isoprene SOA under both high-NO_x and low-NO_x conditions are shown in Fig. 3, Panel b (Surratt et al., 2010; Gomez-Gonzalez et al., 2008; Szmigielski et al., 2007; Surratt et al., 2007, 2006; Claeys et al., 2004; Wang et al., 2005). Surratt et al. (2006) found that under low-NO_x conditions, ~25–30 % of the SOA mass in seeded experiments is organic peroxides, and under high-NO_x conditions, oligomers comprise ~22–34 % of the SOA mass. Oligomerization of both methyltetrols and methylglyceric acid (or peroxides and nitrates thereof) results in the loss of water, especially under low RH condtions and therefore leads to lower H/C and O/C ratios. Products resulting from the linear oligomerization of 2-methyltetrol, 2-methylglyceric acid, and 2-methylglyceric acid nitrate are shown in Fig. 3, Panel b with the oligomerization limits denoted with circles. The locations of the circles highlight the importance of oligomerization in the isoprene system by suggesting that the elemental composition measured by the AMS represents that of highly oligomerized compounds rather than individual monomers or dimers; even better agreement between oligomers and AMS data is possible if one considers crosslinked oligomerization and other dehydration reactions. This observation is consistent with Dommen et al. (2006) who, based on volatility tandem differential mobility analyzer (VTDMA) measurements, found that under lower humidities isoprene SOA volatility is decreased, suggesting the effect of oligomerization.

3.3 Monoaromatic SOA

Figure 4 presents both diagrams for toluene and *m*-xylene photooxidation SOA. Like isoprene and α-pinene photooxidation SOA, toluene and *m*-xylene SOA spectra sit on the right side of the triangle and migrate upwards, likely representing an increase in organic acid content and a decrease in non-acid oxygenates, possibly unsaturated carbonyls. This is consistent with studies showing small organic acids as a major aromatic SOA product (Fisseha et al., 2004). Increasing SOA oxygenation is also apparent in the Van Krevlen diagram as the AMS data show decreasing H/C ratios and increasing O/C ratios with continued oxidation. In addition, both plots show that *m*-xylene SOA is less oxidized than toluene SOA due to the presence of the second methyl group in *m*-xylene.

Structures of identified SOA products from toluene photooxidation are indicated in the Van Krevelen diagram Fig. 4, (Panel b) (Forstner et al., 1997; Hamilton et al., 2005; Sato et al., 2007; Fisseha et al., 2004; Edney et al., 2003; Kleindienst et al., 2004). Despite numerous studies investigating the aerosol composition of aromatic SOA, substantial mass closure has been difficult to achieve. For instance Forstner et al. (1997) studied the molecular composition of SOA formed from the photooxidation of several aromatic compounds and could quantify only 15–30 % of the aerosol mass. In subsequent studies, typically 1 % of toluene SOA could be identified (Hamilton et al., 2005; Sato et al., 2007). A study by Fisseha et al. (2004) determined 20–45 % of SOA from trimethylbenzene photooxidation were small organic acids. The uncertainty in the composition of aromatic SOA

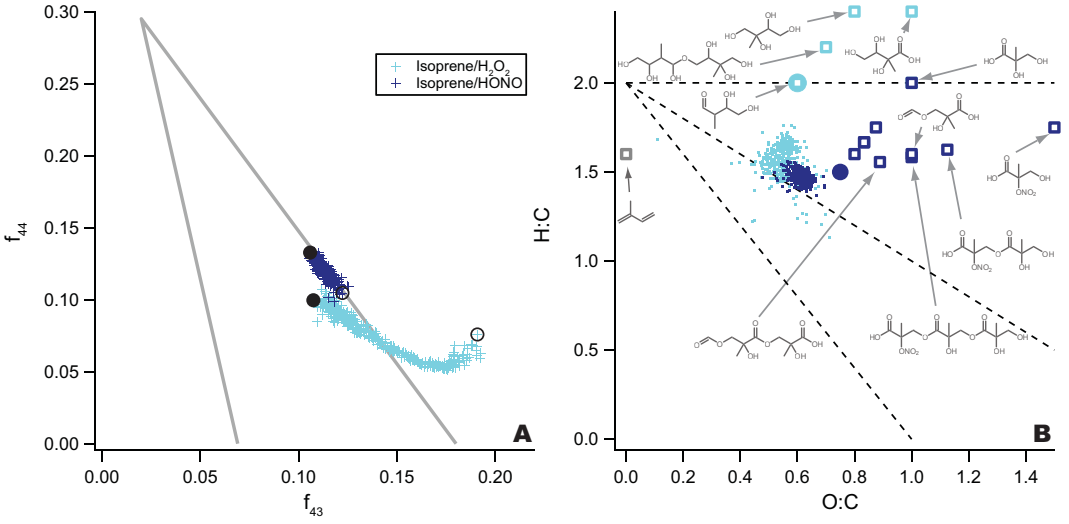

Fig. 3. (A) "Triangle plot" for SOA formed from photooxidation of isoprene under low- and high-NO_x conditions. Open and closed black circles represent the beginning and end of the experiments, respectively. **(B)** Van Krevelen diagram for SOA formed from photooxidation of isoprene under low- and high-NO_x conditions Identified SOA products of each NO_x condition are presented in blue boxes of the corresponding color (Surratt et al., 2006; Claeys et al., 2004; Wang et al., 2005; Surratt et al., 2007; Gomez-Gonzalez et al., 2008). Surratt et al. (2006) found that under low-NO_x conditions, ∼25–30 % of the SOA mass in seeded experiments is organic peroxides, and under high-NO_x conditions, oligomers comprise ∼22–34 % of the SOA mass. Oligomeric limits for each NO_x condition are represented by circles.

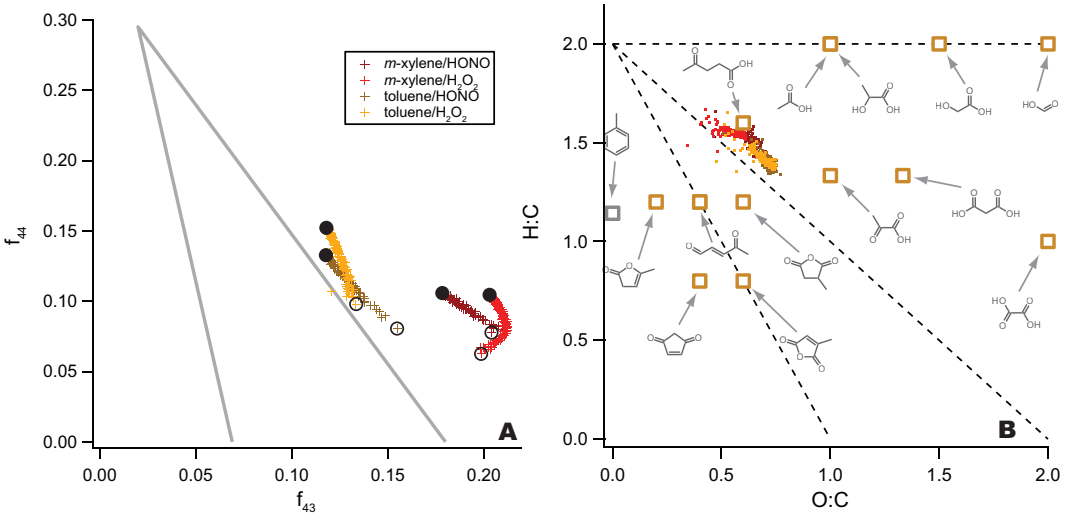

Fig. 4. (A) "Triangle plot" for SOA formed from photooxidation of toluene and *m*-xylene under low- and high-NO_x conditions. Open and closed black circles represent the beginning and end of the experiments, respectively. **(B)** Van Krevelen diagram for SOA formed from photooxidation of isoprene under low- and high-NO_x conditions. Identified toluene-SOA products are presented in tan boxes (Sato et al., 2007; Hamilton et al., 2005; Bloss et al., 2005; Fisseha et al., 2004; Jang and Kamens, 2001; Kleindienst et al., 2004; Edney et al., 2003). Substantial mass closure has been difficult to achieve in molecular characterization studies.

is illustrated by the wide spread of SOA products around the AMS data and the absence of a clear representative compound or process explaining the measured elemental composition. AMS measurements indicate SOA that is less oxidized than the indicated compounds would suggest. However, many of the small acids and carbonyls towards the top of Fig. 4, Panel b, are quite volatile and could represent monomers that have hydrated due to sample analysis. Similarly, compounds towards the bottom left of the figure are anhydrides that may have formed from sample work up.

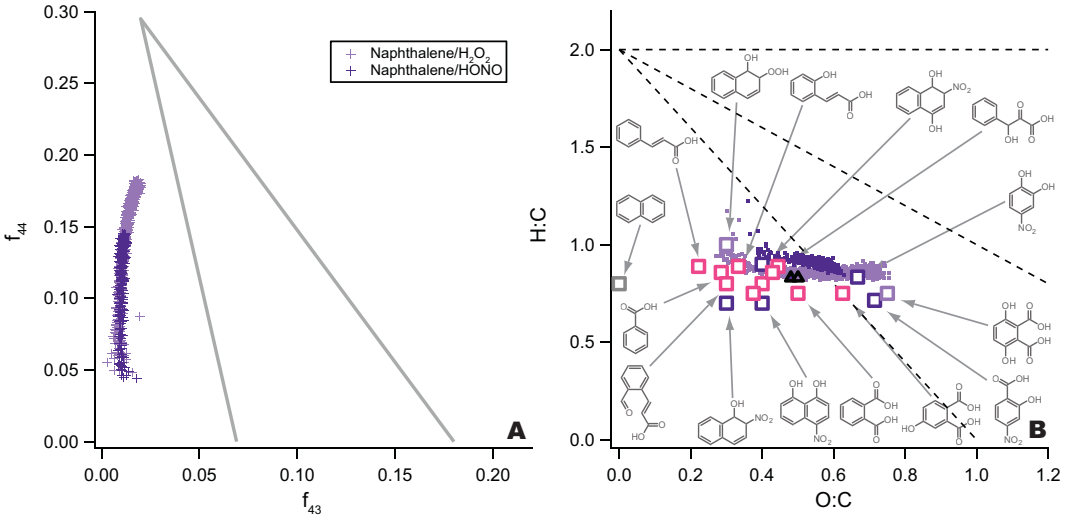

Fig. 5. (A) "Triangle" plot for SOA formed from photooxidation of naphthalene under low- and high-NO_x conditions. Experiment progression is from bottom to top. **(B)** Van Krevelen diagram for SOA formed from photooxidation of isoprene under low- and high-NO_x conditions. Identified SOA products of high-, low-, and both NO_x conditions are presented in dark purple, light purple, and pink boxes, respectively (Kautzman et al., 2009). The mass weighted average H/C and O/C at each NO_x condition are represented by triangles of the same color. Kautzman et al. (2009) were able to chemically characterize 53–68 % of the SOA mass.

This could explain the divergence from AMS data in the Van Krevelen diagram manifested as movement up or down along a line of slope 2.

3.4 Naphthalene SOA

Figure 5 presents the Van Krevelen and "triangle plots" for naphthalene photooxidation SOA. In contrast to the preceeding SOA systems, naphthalene AMS data lie to the left of the "triangle plot" and migrate straight upwards (Panel a), consistent with elemental AMS measurements on the Van Krevelen diagram which show increasing O/C ratios (Panel b). The aromaticity of naphthalene allows for multiple oxidation pathways, including bicyclic peroxy radical and ring-opening routes that lead to substantial organic acid yields. Kautzman et al. (2009) determined that about 16 % of SOA formed under high-NO_x conditions and 33 % of SOA formed under low-NO_x conditions are organic acids. Higher organic acid concentrations under low-NO_x conditions are also consistent with AMS data which exhibit higher f_{44} values and O/C ratios than those of high-NO_x data, likely a result of higher OH exposures (Chhabra et al., 2010).

Structures of SOA products identified by Kautzman et al. (2009) in naphthalene SOA and their elemental compositions are presented in Fig. 5, Panel b. Kautzman et al. (2009) were able to chemically characterize 53–68 % of the SOA mass and Chhabra et al. (2010) found close agreement between the elemental ratios of compounds identified and bulk ratios determined by AMS analysis. The mass weighted elemental compositions of naphthalene SOA formed under low and high NO_x conditions as measured by filter analysis is represented by light and dark purple triangles, respectively. Oxygen-to-carbon ratios of identified species also span a range similar to that of AMS measurements of low-NO_x SOA, evidence of continuous aging.

3.5 Phenol and methoxyphenol SOA

Phenol and methoxyphenol compounds have been investigated as they are semivolatile species formed from the pyrolysis of lignin, the dominant process in biomass burning. Hawthorne et al. (1992) found that phenols and methoxyphenols accounted for forming 21 % and 45 % of aerosol mass from wood smoke, respectively. Like naphthalene SOA, phenol and methoxyphenol SOA lie to the left of the "triangle" with the highest f_{44} values of any precursor studied (Fig. 6a). Similarly, O/C ratios of methoxyphenols range from 0.8 to 1.0; syringol SOA achieves the highest O/C ratios measured for any chamber aerosol precusor system. The O/C values measured here are in close agreement with those of compounds formed in aqueous reactions of phenolic compounds (Sun et al., 2010). Addition of methoxy groups to the phenol ring increases the H/C but tends to lead to decreases of the f_{44} of the resulting SOA. The presence of methoxy groups, while increasing the bulk oxygenation of SOA, may be retained in the SOA and inhibit acid formation.

Proposed structures of detected SOA products from guaiacol photooxidation are indicated in the Van Krevelen diagram (Fig. 6, Panel b). AMS measured elemental composition of SOA generated under high and low-NO_x regimes

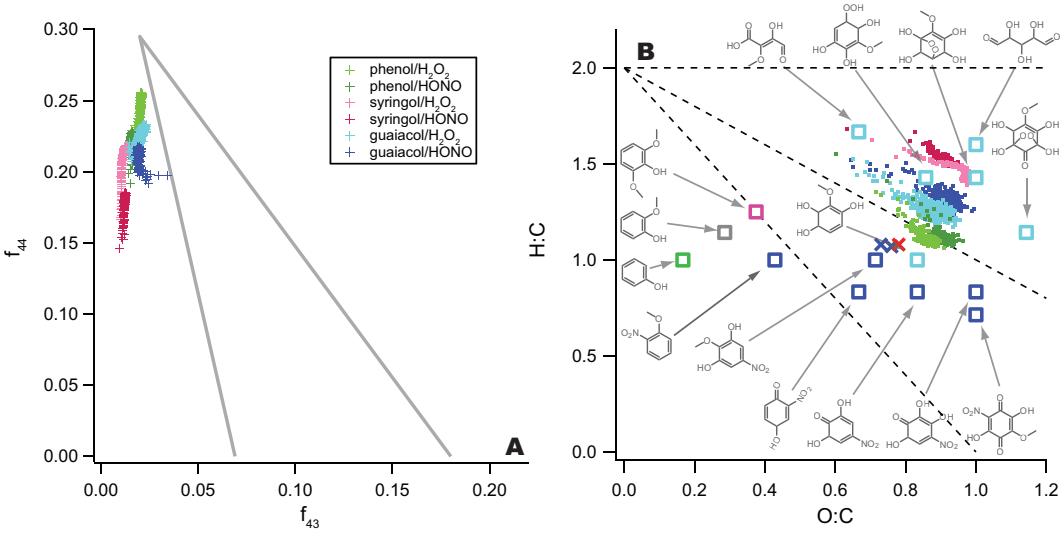

Fig. 6. **(a)** "Triangle plot" for SOA formed from photooxidation of phenol, guaiacol, and syringol under low- and high-NO_x conditions. Experiment progression is from bottom to top. **(B)** Van Krevelen diagram for SOA formed from photooxidation of phenol, guaiacol, and syringol under low- and high-NO_x conditions. Identified guaiacol-SOA products of high- and low-NO_x conditions are presented dark and light blue boxes respectively. Elemental ratios as measured by FTIR data are represented by red (low-NO_x) and blue (high-NO_x) crosses. Quantification of molecular species in methoxyphenol SOA systems has not yet been accomplished.

generally agree with the proposed compounds formed under low-NO_x conditions but have higher H/C ratios than those of compounds formed under high-NO_x conditions. It is possible that the UPLC-MS techniques generally used in conjunction with filter sampling is biased to detect the high-NO_x compounds shown, compounds with lower H/C ratios. It is also possible that much of the SOA mass remains unmeasured by the UPLC-MS technique as much of the SOA could be in the form of small ring opened products (and their oligomers) such as those measured in monoaromatic SOA. This is supported by the large oxygen contribution in CO_2^+ (and other associated ions) in high-resolution AMS spectra as will be discussed in Sect. 3.8.

The FTIR elemental analysis underestimates O/C as compared to the AMS elemental analysis. This maybe a result of the O/C constraint (as described in the Supplement) that is used to parameterize guaiacol SOA changing with oxidation. It is likely that the true parameterization lies somewhere between the ambient case and the precursor-specific case.

3.6 Unsaturated aldehyde SOA

Aldehdyes are widely formed in the atmospheric oxidation of SOA precursors; methacrolein is a gas-phase product of the high-NO_x photooxidation of isoprene. Recent studies have shown that aldehydes are important intermediates to SOA formation and sensitive to NO and NO_2 concentrations (Chan et al., 2010; Surratt et al., 2010). The "triangle plot" and Van Krevelen Diagram for SOA formed from the high-NO_x photooxidation of methacrolein, acrolein, and crotonaldehyde are given in Fig. 7. As shown in Fig. 1, crotonaldehyde and methacrolein are structural isomers of each other while acrolein lacks the additional methyl group. SOA from all three precursors cluster high in the "triangle plot" with acrolein having the highest f_{44} values. Such high oxidation states are likely due to carboxylic acids and esters contributing a larger fraction of the OA mass. This is consistent with acrolein SOA exhibiting the highest O/C ratios (∼0.8) of the three systems. SOA from methacrolein photooxidation has higher f_{43} values than that of crotonaldehyde SOA, implying that the position of the methyl group on the oligomeric chain affects fragmentation in the AMS, but does not change the elemental composiition of the SOA substantially.

Oligomers identified in crotonaldehyde and acrolein SOA are depicted in Fig. 7, Panel b. The monomers and oligomers formed from methacrolein photooxidation are the same as those of high-NO_x isoprene SOA (Surratt et al., 2010). Like isoprene SOA, the addition of each monomer to the oligomeric chain results in the loss of a water molecule. The elemental composition of the limit of a linear oligomer is represented by a circle and approaches the AMS measurement suggesting that the AMS measurement is that of a highly esterified compound rather than individual monomers. As in the isoprene case, the lower O/C ratios measured by the AMS is likely due to the inability of the AMS to efficiently detect oxygen in an organic nitrate group (Farmer et al., 2010; Rollins et al., 2010) as discussed in Sect. 3.9.

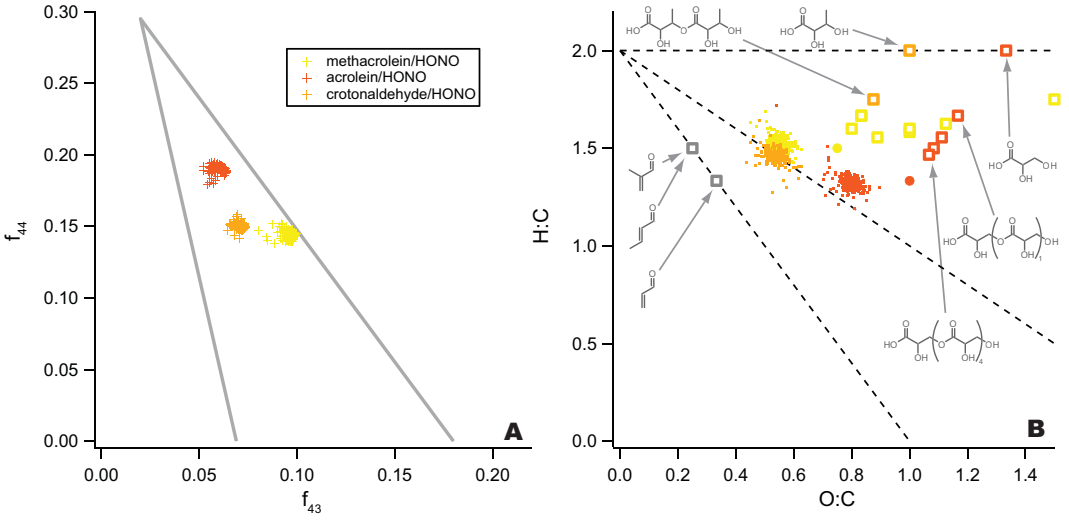

Fig. 7. (A) "Triangle plot" for SOA formed from photooxidation of methacrolein, acrolein, and crotonaldehyde. **(B)** Van Krevelen diagram for SOA formed from photooxidation of methacrolein, acrolein, and crotonaldehyde. Identified SOA products of each system are presented in boxes of the corresponding color (Chan et al., 2010). Oligomeric limits for each system condition are represented by circles.

3.7 SOA from reactive uptake of glyoxal

The reactive uptake of glyoxal onto ammonium sulfate aerosol and the elemental composition of its OA have been described in previous investigations (Galloway et al., 2009; Chhabra et al., 2010). Glyoxal OA exhibits high O/C ratios due to its high oxygen content and its ability to hydrate and polymerize in the aerosol phase (Fig. 8, Panel b). Despite a high measured O/C ratio, glyoxal OA sits on the bottom left of the "triangle plot", a result of insignificant signals at *m/z* 43 and 44. Most of the oxygen signal in glyoxal OA spectra resides in *m/z* 29 (CHO^+), 30 (CH_2O^+), 31 (CH_3O^+), and 47 ($CH_3O_2^+$) (Chhabra et al., 2010).

Structures proposed to form in the aqueous particle phase are shown in Panel b. Hydrated glyoxal has the highest O/C and H/C values; with consecutive additions of glyoxal, water is removed and the oligomer follows a dehydration route with a limit at the same elemental composition of glyoxal itself. Also shown on the Van Krevelen plot is 1H-imidazole-2-carboxaldeyhde, a compound formed from the reaction of glyoxal with ammonium (Chhabra et al., 2010). The AMS elemental composition measurement lies roughly in the middle of the wide range spanned by the proposed species. Further work is needed in characterizing glyoxal OA, its interaction with inorganic species, and the extent of its oligomerization in SOA.

3.8 Oxygen contribution in organonitrate and acid functional groups

Having measurements of the chemical composition of oxidized SOA from different analytical techniques allows for a rich comparison of the oxygen contribution from different functional groups. Table 2 summarizes the fraction of oxygen originating from organonitrate and organic acid functionality in SOA formed at the end of oxidation experiments as determined by AMS, FTIR and speciation techniques. The oxygen contribution to organic acids groups in high-resolution AMS data was calculated by determining the total oxygen mass measured at CO_2^+ as well as those ions dependent on the CO_2^+ signal through the fragmentation table, O^+, HO^+, H_2O^+, and CO^+ (Aiken et al., 2008). The oxygen contribution to organic nitrate groups in AMS data was determined from the total oxygen contribution at NO_x family ions, NO^+ and NO_2^+. Oxygen contribution in acid and nitrate groups are calculated from FTIR measurements by multiplying the measured functional group mass by the mass fraction of oxygen in the group. Contributions of oxygen in speciation studies are calculated similarly but on a species basis.

Table 2 shows that the FTIR, AMS and speciation techniques find that naphthalene and methoxyphenol systems have the greatest fraction of total SOA oxygen in organic acid groups. High-resolution AMS data find that 65–72 % of oxygen signal can be found at acid associated ions in naphthalene SOA formed under high and low-NO_x conditions, respectively. This is in fair agreement with Kautzman et al. (2009) who found 73–81 % of speciated oxygen is contained in acid groups. Further investigation of the AMS data of naphthalene high-NO_x SOA shows that at the peak of SOA growth, the acid-oxygen contribution is only 41 % while the nitrate-oxygen contribution is 22 %. As oxidation continues, the contribution of nitrate-oxygen decreases significantly to 6 % while the acid fraction increases to 65 %, as listed in Table 2. These observations are supported by the data and structures in Fig. 5. SOA formed under both conditions exhibit a

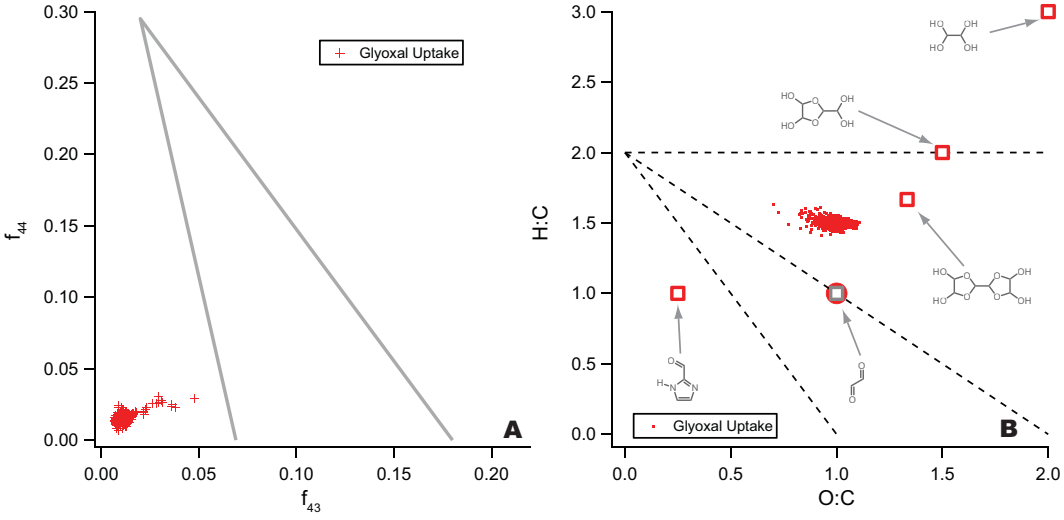

Fig. 8. (A) "Triangle plot" for SOA formed from reactive uptake of glyoxal onto wet ammonium sulfate aerosol. **(B)** Van Krevelen diagram for SOA formed from the uptake of glyoxal onto wet ammonium sulfate aerosol. Proposed SOA products are presented in boxes (Galloway et al., 2009; Kua et al., 2008; Loeffler et al., 2006). Oligomeric limits for glyoxal oligomerization condition is represented by a circle.

steady increase in f_{44} in Panel a and structures in Panel b are overwhelmingly acid while the nitronaphthalene compounds appear at lower O/C ratios corresponding to lower irradiation times. It is possible that under high-NO_x conditions, nitronaphthalene compounds are formed initially but react further to remove nitrogen functionality and add acid functionality. FTIR and AMS data also find significant contributions of oxygen in acid functional groups in guaiacol SOA and relatively small fraction of oxygen in nitrate groups. As was mentioned in Sect. 3.5, much of the SOA could be in the form of small ring-opening products that are typically difficult to separate and identify using UPLC-MS techniques.

In contrast, FTIR and AMS high-resolution data measures significantly less oxygen in acid groups than what was determined from the characterization performed by Yu et al. (1999) and Jaoui and Kamens (2001) for the α-pinene SOA systems. The greatest discrepancy occurs for photooxidation SOA where 31 to 40 % of the AMS measured oxygen occurs at acid associated ions while Jaoui and Kamens (2001) find the fraction of oxygen in acid groups to be 70 %. However, Jaoui and Kamens (2001) do not identify any organonitrates compounds. If the contribution of nitrate-oxygen is removed in FTIR and AMS data, the comparison improves; the FTIR and AMS acid-oxygen contributions become 50 % and 36 %. It is possible that organonitrates may have gone undetected in the characterization performed by Jaoui and Kamens (2001) either through loss in sample work up or poor sensitivity in the GC-EIMS technique used.

The AMS measures a greater contribution of oxygen in acid associated ions for isoprene SOA formed under high-NO_x conditions than under low-NO_x conditions. This can be explained by the abundance of methyl glyceric acids and oligoesters detected in high-NO_x SOA as opposed to the tetrols and polyols in low-NO_x SOA. In high-NO_x SOA spectra, nitrate ions contribute 8 % of the total oxygen signal while nitrate groups in the structures depicted in Fig. 3, Panel b exhibit a much larger nitrate contribution. This is possibly explained by the inability of the AMS to fully detect oxygen in organonitrates compounds, as is discussed in Sect. 3.9. This would also explain the low contribution of oxygen in nitrate ions for the spectra of unsaturated aldehyde SOA. High-resolution AMS spectra exhibit an acid-oxygen contribution of 37–50 % and a nitrate-oxygen contribution of 10–14 % for monoaromatic SOA. While the oxygen fraction in nitrate ions decreases slightly over time, it still represents a significant contribution to the measured AMS O/C. It is possible that organic nitrogen is present in particle-phase ring-opening products that are not easily separated or identified through offline methods more work needs to be done to characterize aromatic SOA and determine what effect sample preparation and analysis can have on the measurement.

3.9 AMS analysis uncertainty

Much of the uncertainty in AMS analysis data can be attributed to the treatment of organonitrate compounds. In ambient data sets, nitrate is generally considered inorganic and therefore NO_x family ions (NO^+ and NO_2^+) are not included as part of the organic elemental analysis, possibly leading to underestimation of ambient SOA O/C values. Farmer et al.

Table 2. Fraction SOA oxygen contribution in organic acid, organic nitrate, and other functionalities as measured by the AMS, FTIR, and speciation analyses.

		Oxygen Contribution		
SOA System	Measurement Method	Acid[a]	Nitrate[b]	Other
α-pinene ozonolysis				
	AMS	0.41	0.00	0.59
	Yu et al. (1999)	0.58	0.00	0.42
α-pinene photooxidation				
	AMS low-NO_x	0.31	0.00	0.69
	FTIR low-NO_x	0.31	0.00	0.69
	AMS high-NO_x	0.33	0.10	0.58
	FTIR high-NO_x	0.40	0.19	0.41
	Jaoui and Kamens (2001)	0.70	0.00	0.30
isoprene photooxidation				
	AMS low-NO_x	0.37	0.00	0.63
	AMS high-NO_x	0.45	0.09	0.47
monoaromatic photooxidation				
	toluene AMS low-NO_x	0.50	0.00	0.50
	toluene AMS high-NO_x	0.42	0.10	0.48
	m-xylene AMS low-NO_x	0.37	0.00	0.63
	m-xylene AMS high-NO_x	0.36	0.14	0.49
naphthalene photooxidation				
	AMS low-NO_x	0.72	0.00	0.28
	Kautzman et al. (2009) low-NO_x	0.82	0.00	0.18
	AMS high-NO_x	0.65	0.06	0.29
	Kautzman et al. (2009) high-NO_x	0.73	0.07	0.20
methoxyphenol photooxidation				
	phenol AMS low-NO_x	0.77	0.00	0.23
	phenol AMS high-NO_x	0.69	0.04	0.27
	guaiacol AMS low-NO_x	0.61	0.00	0.39
	guaiacol FTIR low-NO_x	0.77	0.00	0.23
	guaiacol AMS high-NO_x	0.70	0.06	0.24
	guaiacol FTIR high-NO_x	0.82	0.01	0.18
	syringol AMS low-NO_x	0.59	0.00	0.41
	syringol AMS high-NO_x	0.54	0.04	0.42
unsaturated aldehyde photooxidation				
	acrolein AMS high-NO_x	0.54	0.04	0.42
	methacrolein AMS high-NO_x	0.55	0.04	0.41
	crotonaldehyde AMS high-NO_x	0.50	0.03	0.47

[a] Oxygen contribution to organic acids groups in high-resolution AMS data was calculated by determining the total organic oxygen mass measured at CO_2^+, O^+, HO^+, H_2O^+, and CO^+ (Aiken et al., 2008).
[b] Oxygen contribution to organic acids groups in high-resolution AMS data was calculated by determining the total oxygen mass measured at NO_2^+ and NO^+.

(2010) estimated that for the Study of Organic Aerosols in Riverside (SOAR-1) ambient campaign, organonitrates contribute 5–10 % of the total nitrate mass, though do not dominate AMS nitrate spectra. In the analysis of high-NO_x chamber experiments in which the humidity is too low for nitrate acid to appreciably partition to the particle phase, categorizing NO_x family ions as organic is an appropriate assumption to make. However, even when NO_x family ions are included

as part of the total organic mass spectra, their oxygen contribution tends to be underestimated due to the inability of the AMS to detect the nitrogen-bonded oxygen in the $-ONO_2$ group (Farmer et al., 2010; Rollins et al., 2010). This may also occur for peroxides formed under low-NO_x conditions; upon fragmentation the RO-OH bond can sever leaving the OH fragment effectively undetected. This maybe a reason why SOA formed under different NO_x regimes have similar elemental compositions. On average, inclusion of NO_x family ions to the organic spectra increases the O/C ratio of the systems studied by 0.05, with *m*-xylene SOA having the largest difference of 0.10 and crotonaldehyde having the smallest difference of 0.02. These contributions also tend to decrease as a function of experiment time. Thus, the relative formation of organonitrates is precursor and time dependent and, therefore, so is the contribution of NO_x family ions to the O/C. However, these differences still fall within the uncertainty reported by Aiken et al. (2008). Organonitrate oxygen is included fully in the calculation of O/C for speciated measurements. However, the detection and quantification of organonitrate compounds is again system dependent. Despite these limitations, we still see that for systems in which SOA can be chemically characterized well, the AMS and average speciated O/C agree. As detection and quantification techniques of organonitrates improve, more robust comparisons between measurement techniques can be achieved, and the contribution of organic nitrogen to ambient SOA can be better constrained.

Another source of uncertainty is the calibration factors and fragmentation table ratios used to correct for ionization biases in AMS spectra and air contamination. The applied correction factors are based on a limited set of standards and have an inherent uncertainty (Aiken et al., 2008). As was discussed by Chhabra et al. (2010), these standards are large alkanols, alkanoic acids, and aromatic species that are similar to those detected in α-pinene and naphthalene SOA. By contrast, few of the standards have structures similar to species found in isoprene and aromatic SOA like polyols and small acids. Kessler et al. (2010) has shown that for polyhydroxylated species, the default correction factor for O/C underestimates O/C.

There is also uncertainty in the AMS fragmentation table particularly when determining the relative contribution of CO^+, H_2O^+, and CO_2^+ ions in high-resolution spectra. As shown in the supplemental section, the ratio of organic CO^+ to CO_2^+ was found to be close to unity, the default fragmentation wave value based on Aiken et al. (2008), so this value was used. In a study by Chen et al. (2011), researchers determined fragmentation ratios much different than those measured by Aiken et al. (2008) for the isoprene low-NO_x photooxidation system. Using those ratios to calculate O/C ratios for the low-NO_x isoprene SOA system presented here increases the O/C by 57 %. More work is needed to constrain these ratios in both ambient and chamber environments.

4 Discussion and conclusions

We investigate two different analysis methods ("triangle plot" and Van Krevelen diagram) for representing the general processes of formation and aging of SOA. Figure 9 summarizes SOA data in a "triangle plot" and Van Krevelen diagram for the variety of laboratory systems studied. Despite the variety of experimental conditions, differences in oxidative conditions have relatively little effect on the spectral identity and elemental composition of SOA as measured by the AMS compared to the identity of the SOA precursor. Most SOA formed under high- and low-NO_x conditions occupy similar areas in the "triangle plot" and Van Krevelen diagram. Typically, chemical characterizations of SOA find signficant concentrations of peroxides under low-NO_x conditions and organic nitrates under high-NO_x conditions. However, it is likely that these differences in functionality do not lead to substantial differences in f_{43} and f_{44} and the elemental composition as the underlying chemical structure of SOA remains relatively unchanged and because the AMS has difficulty in measuring oxygen that is lost in fragmented organic nitrate and peroxide functionality. All individual photooxidation systems, apart from the aldehydes whose carbon chain is too small to support continued oxidation without fragmentation into more volatile species, also show that AMS spectra head toward the top of the "triangle plot" as they age, consistent with an increase in O/C ratios in the Van Krevelen diagram. Evidence from other AMS studies suggest that this movement toward the top of the "triangle plot" is representative of an increase in organic acids (Alfarra, 2004; Aiken et al., 2007; Takegawa et al., 2007; Duplissy et al., 2011).

We find general agreement between the f_{43} and f_{44} values presented in Ng et al. (2010) and those presented here for the traditional set of SOA systems: monoaromatic, α-pinene, and isoprene SOA. In cases where f_{43} and f_{43} differ by more than 2 % are possibly due to differences in organic loading; Shilling et al. (2009) found that f_{43} increased with increasing loading. Differences in f_{43} and f_{44} could also result from differences in vaporizer temperature leading to small differences in spectral signal at low *m/z* These SOA systems cluster in the lower half of the "triangle plot" indicating relatively low oxygen content and a high degree of mass spectral variation, similar to SV-OOA components. The additional SOA precursors studied here exhibit more mass spectral variation and show that highly oxidized OA with similar O/C ratios to LV-OOA can be formed in a laboratory chamber. The most oxidized SOA formed in the systems studied here results from the photooxidation of already oxidized VOCs, methoxyphenols and unsaturated aldehydes, suggesting that OH exposure is the limiting variable in SOA oxidation. The OH exposure for the photooxidative experiments vary from 1 to 2×10^9 molec cm^{-3} min which is equivalent to approximately 1–2 days in the ambient atmosphere. In contrast, Lambe et al. (2011) report minimum and maximum OH exposures of 1×10^{11} and 2×10^{12} molec cm^{-3} s, respectively,

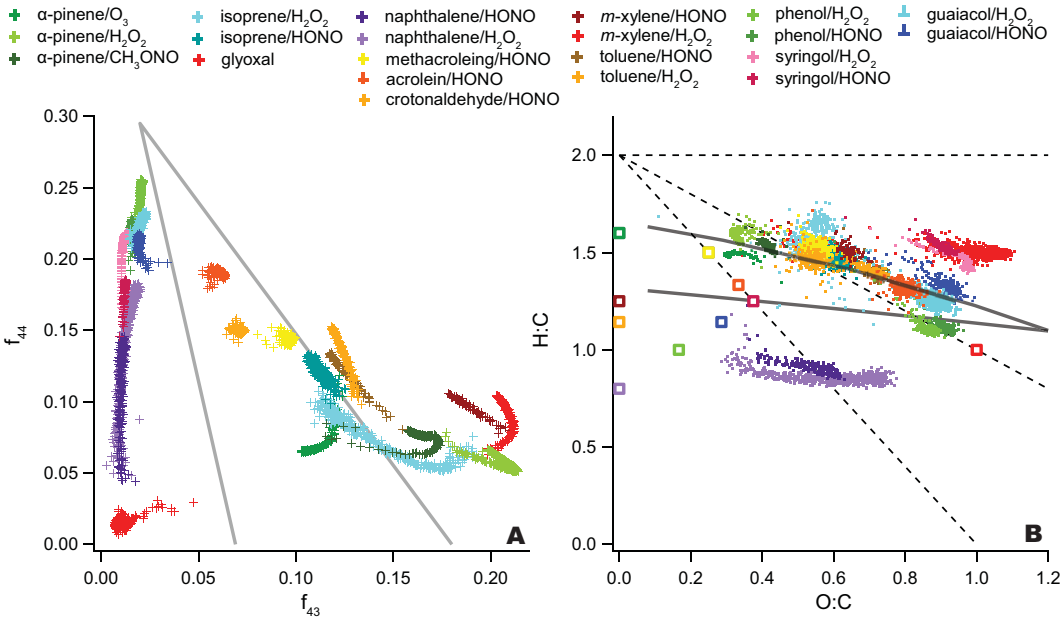

Fig. 9. **(A)** Triangle plot for all SOA systems **(B)** Van Krevelen diagram for all SOA systems. SOA precursors are represented by corresponding colored boxes. The "VK-triangle" parameterization developed by Ng et al. (2011) is represented by solid gray curves.

for Potential Aerosol Mass (PAM) flow tube experiments, corresponding to 1 to 23 days in the ambient atmosphere. The much higher OH exposures allow Lambe et al. (2011) to start with SOA at the bottom of the "triangle plot" and move all the way to the top. While f_{44} has the ability to increase significantly in chamber experiments (naphthalene for example), movement from the bottom of the triangle with a single precursor is not possible with the smaller OH exposures. To account for this, already oxidized precursors can be used as surrogates for creating highly oxidized SOA as seen in the methacrolein and isoprene high-NO_x systems. Methacrolein, a gas-phase product and major SOA intermediate of isoprene photooxidation that forms when the isoprene hydroxyperoxy radical reacts with NO, yields SOA with f_{43} and f_{44} values just beyond those of isoprene SOA range. It is likely that isoprene SOA formed under high-NO_x conditions falls short of methacrolein SOA in the "triangle plot" because the isoprene SOA would also include products that form from RO_2-HO_2 reactions that occur at lower NO_x concentrations. In the extreme case, methoxyphenol SOA simulates the continued oxidation of napthalene SOA and is subject to multiple oxidation steps on an already oxidized compound, leading to O/C ratios that approach unity. Although containing aromatic functionality, both methoxyphenols and naphthalene generate SOA spectra that group on the left side of the "triangle plot" while *m*-xylene and toluene generate SOA spectra that group on the right side. Similarly, Ng et al. (2010) found that benzene SOA spectra sit on the left side of the "triangle plot" and 1,3,5-trimethylbenzene SOA spectra sit on the right. It is likely that functionality on the aromatic ring of the SOA precursor affects the fragmentation of the resultant SOA. Specifically, groups like $-CH_3$ on the aromatic ring yield SOA spectra with high f_{43} values while electron donating groups like $-OH$ and $-OCH_3$ or the lack of functionality on the aromatic ring yield SOA spectra with low f_{43} values. Table 2 shows that while nitrate and acid groups contain much of the oxygen in oxidized SOA, a similar fraction remains in other ions such as $C_2H_3O^+$ at *m/z* 43. More work needs to be done to quantify these non-acid, non-nitrate oxygenated functionalities and determine how they fragment to form AMS spectra.

Figure 9, Panel b demonstrates that change in elemental composition that occurs from SOA precursor to SOA is a function of the precursor identity and structure. α-pinene ozonolysis SOA exhibits the smallest change in O/C because ozone is only reactive to alkene functionality, and once the double bond in α-pinene has reacted, the potential for aging through ozonolysis is halted. OH radicals will react with saturated aliphatic carbon but to a much lesser extent than alkene functionality so further oxidation is dramatically slowed. Aromatics, however, show much greater potential for increases in O/C because aromaticity allows many more oxidative steps starting with OH attack to bicyclic radical formation, to ring cleaving. Both naphthalene and phenol undergo large changes in O/C as the unsaturated rings add oxygen. In the case of naphthalene, H:C remains low because OH cleaves one ring at a time leaving one aromatic ring intact. For phenol, the H:C is higher due to the fact

that the monoaromatic ring opens allowing for OH radicals to saturate double bonds.

The Van Krevelen diagrams of the elemental composition of individual SOA systems reveal that elemental ratios measured by the AMS agree most closely with SOA systems for which the greatest degree of mass closure has been achieved, within the uncertainty of the AMS elemental analysis. Yu et al. (1999) were able to speciate >90 % of the α-pinene ozonolysis aerosol composition by mass, and Kautzman et al. (2009) were able to characterize 53–68 % of the SOA formed from naphthalene photooxidation, the two systems with the closest agreement between measured elemental ratios and identified compounds. The diagrams also illustrate that highly oligomerized compounds may dominate, in particular, SOA systems such as isoprene and unsaturated aldehyde photooxidation. Conversely, in systems for which mass closure has been difficult, such as monoaromatics, AMS and filter data do not agree.

From a variety of ambient and laboratory measurements, Heald et al. (2010) found that atmospheric OA occupy a narrow range in the Van Krevelen diagram following a line with slope of -1 implying the addition of carboxylic acids or equal amounts of hydroxy and carbonyl functional groups on average to a saturated carbon chain. From Fig. 9, Panel b, the set of SOA systems on the Van Krevelen diagram tend to map a slope shallower than -1. In the systems studied here, most SOA precursors do not resemble a saturated chain, and many have cyclic chains, alkene, or aromatic groups. This allows for oxidation of the precursor without substantial loss of hydrogen, leading to a slope shallower than -1, even with the addition of carbonyl and acid groups. Aging pathways on the Van Krevelen diagram are likely to be different for different precursor species like isoprene and α-pinene and for different precursor classes like biogenic and anthropogenic VOCs. Recently Ng et al. (2011) developed a parameterization to transform ambient OOA components in the "triangle plot" directly onto the Van Krevelen space. The transformed ambient "VK-triangle" (shown in Fig. 9, Panel b) is consistent with the chamber data and also yields a slope shallower than -1.

Figure 9, Panel a shows that precursor structure and functionality determine the SOA "starting point" on the "triangle plot" and that the path taken is largely dependent on identity of the SOA precursor. Ng et al. (2010) showed that as SOA photochemically ages, and becomes more oxidized, spectral uniqueness is lost and SOA on the "triangle plot" becomes chemically similar. Panel a supports this model with higher f_{44} values correlating with increased SOA oxygenation and a tendency for SOA to converge towards the peak of the triangle, which corresponds to an oxidation state ($\overline{OS_C} \approx 2 \times O/C - H/C$) (Kroll et al., 2011) of around 1 (Ng et al., 2011; Kroll et al., 2011). Panel a also shows that with a finite set of SOA precursors, one can essentially recreate the "triangle plot" as originally created by Ng et al. (2010). The SOA spectra represented on the boundaries of the triangle do not mean that they are not representative of ambient spectral components nor do they represent the spectral extremes of chamber SOA as the complete set of SOA precursors is far from being known. Rather this SOA lies along the outlines of the triangle depicted by Ng et al. (2010). Ambient spectra and components falling within the triangle represent the ensemble average of many different SOA precursors and oxidative processes that mix spatially and temporally. And as SOA becomes more oxidized, it loses its source history. Recently, work by Lee et al. (2011) show that oxidized solutions of pinonic acid, glyoxal and SOA from laboratory and ambient sources map out a larger triangular area than what was depicted by Ng et al. (2010) and that mixing aerosol sources also mixed their spectra signals. Additionally, Lambe et al. (2011) show that the "triangle plot" could be expanded with Potential Aerosol Mass measurements, and those systems that individually lie on the edges of the triangle could be mixed to form SOA that falls in the center of the triangle. Indeed more chamber experiments would help to more fully characterize the "triangle plot" space. High-resolution analysis with species identification can more accurately assign functional groups to individual ions in the AMS spectra. Molecular level chemical characterization of SOA will also be useful in comparison to AMS elemental measurements, especially in systems for which mass closure has been difficult.

Supplementary material related to this article is available online at: http://www.atmos-chem-phys.net/11/8827/2011/acp-11-8827-2011-supplement.pdf.

Acknowledgements. This work was supported by the US Department of Energy Biological and Environmental Research grant DE-FG02-05ER63983, US Environmental Protection Agency STAR grant RD-83374901, and US NSF grant ATM-0432377. It has not been formally reviewed by EPA. The views expressed in this document are solely those of the authors and the EPA does not endorse any products in this publication. The authors would like to thank Christine Loza for SOA yield analysis and Man Nin Chan, Lindsay Yee, and Katherine Schilling for guaiacol filter analysis. The authors would also like to thank Satoshi Takahama for helpful discussions on FTIR analysis.

Edited by: G. McFiggans

References

Aiken, A. C., DeCarlo, P. F., and Jimenez, J. L.: Elemental analysis of organic species with electron ionization high-resolution mass spectrometry, Anal. Chem., 79, 8350–8358, doi:10.1021/Ac071150w, 2007.

Aiken, A. C., Decarlo, P. F., Kroll, J. H., Worsnop, D. R., Huffman, J. A., Docherty, K. S., Ulbrich, I. M., Mohr, C., Kimmel, J. R., Sueper, D., Sun, Y., Zhang, Q., Trimborn, A., Northway,

M., Ziemann, P. J., Canagaratna, M. R., Onasch, T. B., Alfarra, M. R., Prevot, A. S. H., Dommen, J., Duplissy, J., Metzger, A., Baltensperger, U., and Jimenez, J. L.: O/C and OM/OC ratios of primary, secondary, and ambient organic aerosols with high-resolution time-of-flight aerosol mass spectrometry, Environ. Sci. Technol., 42, 4478–4485, doi:10.1021/Es703009q, 2008.

Aiken, A. C., Salcedo, D., Cubison, M. J., Huffman, J. A., DeCarlo, P. F., Ulbrich, I. M., Docherty, K. S., Sueper, D., Kimmel, J. R., Worsnop, D. R., Trimborn, A., Northway, M., Stone, E. A., Schauer, J. J., Volkamer, R. M., Fortner, E., de Foy, B., Wang, J., Laskin, A., Shutthanandan, V., Zheng, J., Zhang, R., Gaffney, J., Marley, N. A., Paredes-Miranda, G., Arnott, W. P., Molina, L. T., Sosa, G., and Jimenez, J. L.: Mexico City aerosol analysis during MILAGRO using high resolution aerosol mass spectrometry at the urban supersite (T0) - Part 1: Fine particle composition and organic source apportionment, Atmos. Chem. Phys., 9, 6633–6653, doi:10.5194/acp-9-6633-2009, 2009.

Alfarra, M. R.: Insights into the atmospheric organic aerosols using an aerosol mass spectrometer, Ph.D. thesis, University of Manchester, Manchester, UK, 2004.

Allan, J. D., Delia, A. E., Coe, H., Bower, K. N., Alfarra, M. R., Jimenez, J. L., Middlebrook, A. M., Drewnick, F., Onasch, T. B., Canagaratna, M. R., Jayne, J. T., and Worsnopf, D. R.: A generalised method for the extraction of chemically resolved mass spectra from aerodyne aerosol mass spectrometer data, J. Aerosol Sci., 35, 909–922, doi:10.1016/j.jaerosci.2004.02.007, 2004.

Bahreini, R., Keywood, M. D., Ng, N. L., Varutbangkul, V., Gao, S., Flagan, R. C., Seinfeld, J. H., Worsnop, D. R., and Jimenez, J. L.: Measurements of secondary organic aerosol from oxidation of cycloalkenes, terpenes, and m-xylene using an Aerodyne aerosol mass spectrometer, Environ. Sci. Technol., 39, 5674–5688, doi:10.1021/Es048061a, 2005.

Bateman, A. P., Nizkorodov, S. A., Laskin, J., and Laskin, A.: Time-resolved molecular characterization of limonene/ozone aerosol using high-resolution electrospray ionization mass spectrometry, Phys. Chem. Chem. Phys., 11, 7931–7942, doi:10.1039/B905288g, 2009.

Bloss, C., Wagner, V., Jenkin, M. E., Volkamer, R., Bloss, W. J., Lee, J. D., Heard, D. E., Wirtz, K., Martin-Reviejo, M., Rea, G., Wenger, J. C., and Pilling, M. J.: Development of a detailed chemical mechanism (MCMv3.1) for the atmospheric oxidation of aromatic hydrocarbons, Atmos. Chem. Phys., 5, 641–664, doi:10.5194/acp-5-641-2005, 2005.

Canagaratna, M. R., Jayne, J. T., Jimenez, J. L., Allan, J. D., Alfarra, M. R., Zhang, Q., Onasch, T. B., Drewnick, F., Coe, H., Middlebrook, A., Delia, A., Williams, L. R., Trimborn, A. M., Northway, M. J., DeCarlo, P. F., Kolb, C. E., Davidovits, P., and Worsnop, D. R.: Chemical and microphysical characterization of ambient aerosols with the aerodyne aerosol mass spectrometer, Mass Spectrom. Rev., 26, 185–222, doi:10.1002/Mas.20115, 2007.

Chan, A. W. H., Kautzman, K. E., Chhabra, P. S., Surratt, J. D., Chan, M. N., Crounse, J. D., Kurten, A., Wennberg, P. O., Flagan, R. C., and Seinfeld, J. H.: Secondary organic aerosol formation from photooxidation of naphthalene and alkylnaphthalenes: implications for oxidation of intermediate volatility organic compounds (IVOCs), Atmos. Chem. Phys., 9, 3049–3060, doi:10.5194/acp-9-3049-2009, 2009.

Chan, A. W. H., Chan, M. N., Surratt, J. D., Chhabra, P. S., Loza, C. L., Crounse, J. D., Yee, L. D., Flagan, R. C., Wennberg, P. O., and Seinfeld, J. H.: Role of aldehyde chemistry and NO_x concentrations in secondary organic aerosol formation, Atmos. Chem. Phys., 10, 7169–7188, doi:10.5194/acp-10-7169-2010, 2010.

Chen, Q., Liu, Y., Donahue, N. M., Shilling, J. E., and Martin, S. T.: Particle-phase chemistry of secondary organic material: Modeled compared to measured O:C and H:C elemental ratios provide constraints, Environ. Sci. Technol., 45, 4763–4770, doi:10.1021/es104398s, 2011.

Chhabra, P. S., Flagan, R. C., and Seinfeld, J. H.: Elemental analysis of chamber organic aerosol using an aerodyne high-resolution aerosol mass spectrometer, Atmos. Chem. Phys., 10, 4111–4131, doi:10.5194/acp-10-4111-2010, 2010.

Claeys, M., Graham, B., Vas, G., Wang, W., Vermeylen, R., Pashynska, V., Cafmeyer, J., Guyon, P., Andreae, M. O., Artaxo, P., and Maenhaut, W.: Formation of secondary organic aerosols through photooxidation of isoprene, Science, 303, 1173–1176, doi:10.1126/science.1092805, 2004.

Cocker, D. R., Flagan, R. C., and Seinfeld, J. H.: State-of-the-art chamber facility for studying atmospheric aerosol chemistry, Environ. Sci. Technol., 35, 2594–2601, doi:10.1021/Es0019169, 2001.

Day, D. A., Liu, S., Russell, L. M., and Ziemann, P. J.: Organonitrate group concentrations in submicron particles with high nitrate and organic fractions in coastal southern California, Atmos. Environ., 44, 1970–1979, doi:10.1016/j.atmosenv.2010.02.045, 2010.

De Gouw, J. and Jimenez, J. L.: Organic Aerosols in the Earth's Atmosphere, Environ. Sci. Technol., 43, 7614–7618, doi:10.1021/Es9006004, 2009.

DeCarlo, P. F., Kimmel, J. R., Trimborn, A., Northway, M. J., Jayne, J. T., Aiken, A. C., Gonin, M., Fuhrer, K., Horvath, T., Docherty, K. S., Worsnop, D. R., and Jimenez, J. L.: Field-deployable, high-resolution, time-of-flight aerosol mass spectrometer, Anal. Chem., 78, 8281–8289, doi:10.1021/Ac061249n, 2006.

Docherty, K. S., Wu, W., Lim, Y. B., and Ziemann, P. J.: Contributions of organic peroxides to secondary aerosol formed from reactions of monoterpenes with O-3, Environ. Sci. Technol., 39, 4049–4059, doi:10.1021/Es050228s, 2005.

Dommen, J., Metzger, A., Duplissy, J., Kalberer, M., Alfarra, M. R., Gascho, A., Weingartner, E., Prevot, A. S. H., Verheggen, B., and Baltensperger, U.: Laboratory observation of oligomers in the aerosol from isoprene/NO_x photooxidation, Geophys. Res. Lett., 33, L13805, doi:10.1029/2006gl026523, 2006.

Donahue, N. M., Robinson, A. L., and Pandis, S. N.: Atmospheric organic particulate matter: From smoke to secondary organic aerosol, Atmos. Environ., 43, 94–106, doi:10.1016/j.atmosenv.2008.09.055, 2009.

Duplissy, J., DeCarlo, P. F., Dommen, J., Alfarra, M. R., Metzger, A., Barmpadimos, I., Prevot, A. S. H., Weingartner, E., Tritscher, T., Gysel, M., Aiken, A. C., Jimenez, J. L., Canagaratna, M. R., Worsnop, D. R., Collins, D. R., Tomlinson, J., and Baltensperger, U.: Relating hygroscopicity and composition of organic aerosol particulate matter, Atmos. Chem. Phys., 11, 1155–1165, doi:10.5194/acp-11-1155-2011, 2011.

Edney, E. O., Kleindienst, T. E., Conver, T. S., McIver, C. D., Corse, E. W., and Weathers, W. S.: Polar organic oxygenates in $PM_{2.5}$ at a southeastern site in the United States, Atmos. Environ., 37,

3947–3965, doi:10.1016/S1352-2310(03)00461-8, 2003.

Farmer, D. K., Matsunaga, A., Docherty, K. S., Surratt, J. D., Seinfeld, J. H., Ziemann, P. J., and Jimenez, J. L.: Response of an aerosol mass spectrometer to organonitrates and organosulfates and implications for atmospheric chemistry, P Natl Acad Sci USA, 107, 6670–6675, doi:10.1073/pnas.0912340107, 2010.

Fisseha, R., Dommen, J., Sax, M., Paulsen, D., Kalberer, M., Maurer, R., Hofler, F., Weingartner, E., and Baltensperger, U.: Identification of organic acids in secondary organic aerosol and the corresponding gas phase from chamber experiments, Anal. Chem., 76, 6535–6540, doi:10.1021/Ac048975f, 2004.

Forstner, H. J. L., Flagan, R. C., and Seinfeld, J. H.: Secondary organic aerosol from the photooxidation of aromatic hydrocarbons: Molecular composition, Environ. Sci. Technol., 31, 1345–1358, doi:10.1021/es9605376, 1997.

Galloway, M. M., Chhabra, P. S., Chan, A. W. H., Surratt, J. D., Flagan, R. C., Seinfeld, J. H., and Keutsch, F. N.: Glyoxal uptake on ammonium sulphate seed aerosol: reaction products and reversibility of uptake under dark and irradiated conditions, Atmos. Chem. Phys., 9, 3331–3345, doi:10.5194/acp-9-3331-2009, 2009.

Gao, S., Keywood, M., Ng, N. L., Surratt, J., Varutbangkul, V., Bahreini, R., Flagan, R. C., and Seinfeld, J. H.: Low-molecular-weight and oligomeric components in secondary organic aerosol from the ozonolysis of cycloalkenes and α-pinene, J. Phys. Chem. A, 108, 10 147–10 164, doi:10.1021/jp047466e, 2004.

Goldstein, A. H. and Galbally, I. E.: Known and unexplored organic constituents in the earth's atmosphere, Environ. Sci. Technol., 41, 1514–1521, doi:10.1021/es072476p, 2007.

Gomez-Gonzalez, Y., Surratt, J. D., Cuyckens, F., Szmigielski, R., Vermeylen, R., Jaoui, M., Lewandowski, M., Offenberg, J. H., Kleindienst, T. E., Edney, E. O., Blockhuys, F., Van Alsenoy, C., Maenhaut, W., and Claeys, M.: Characterization of organosulfates from the photooxidation of isoprene and unsaturated fatty acids in ambient aerosol using liquid chromatography/(-) electrospray ionization mass spectrometry, J. Mass Spectrom., 43, 371–382, doi:10.1002/Jms.1329, 2008.

Hall, W. A. and Johnston, M. V.: Oligomer Content of α-pinene secondary organic aerosol, Aerosol Sci. Tech., 45, 37–45, doi:10.1080/02786826.2010.517580, 2011.

Hallquist, M., Wenger, J. C., Baltensperger, U., Rudich, Y., Simpson, D., Claeys, M., Dommen, J., Donahue, N. M., George, C., Goldstein, A. H., Hamilton, J. F., Herrmann, H., Hoffmann, T., Iinuma, Y., Jang, M., Jenkin, M. E., Jimenez, J. L., Kiendler-Scharr, A., Maenhaut, W., McFiggans, G., Mentel, T. F., Monod, A., Prevot, A. S. H., Seinfeld, J. H., Surratt, J. D., Szmigielski, R., and Wildt, J.: The formation, properties and impact of secondary organic aerosol: current and emerging issues, Atmos. Chem. Phys., 9, 5155–5236, doi:10.5194/acp-9-5155-2009, 2009.

Hamilton, J. F., Webb, P. J., Lewis, A. C., and Reviejo, M. M.: Quantifying small molecules in secondary organic aerosol formed during the photo-oxidation of toluene with hydroxyl radicals, Atmos. Environ., 39, 7263–7275, doi:10.1016/j.atmosenv.2005.09.006, 2005.

Hawthorne, S. B., Miller, D. J., Langenfeld, J. J., and Krieger, M. S.: Pm-10 High-Volume Collection and Quantitation of Semivolatile and Nonvolatile Phenols, Methoxylated Phenols, Alkanes, and Polycyclic Aromatic-Hydrocarbons from Winter Urban Air and Their Relationship to Wood Smoke Emissions, Environ. Sci. Technol., 26, 2251–2262, doi:10.1021/es00035a026, 1992.

Heald, C. L., Kroll, J. H., Jimenez, J. L., Docherty, K. S., DeCarlo, P. F., Aiken, A. C., Chen, Q., Martin, S. T., Farmer, D. K., and Artaxo, P.: A simplified description of the evolution of organic aerosol composition in the atmosphere, Geophys. Res. Lett., 37, L08 803, doi:10.1029/2010gl042737, 2010.

Jang, M. S. and Kamens, R. M.: Characterization of secondary aerosol from the photooxidation of toluene in the presence of NO_x and 1-propene, Environ. Sci. Technol., 35, 3626–3639, doi:10.1021/Es010676+, 2001.

Jaoui, M. and Kamens, R. M.: Mass balance of gaseous and particulate products analysis from alpha-pinene/NO_x/air in the presence of natural sunlight, J. Geophys. Res.-Atmos., 106, 12 541–12 558, doi:10.1029/2001JD900005, 2001.

Jayne, J. T., Leard, D. C., Zhang, X. F., Davidovits, P., Smith, K. A., Kolb, C. E., and Worsnop, D. R.: Development of an aerosol mass spectrometer for size and composition analysis of submicron particles, Aerosol Sci. Technol., 33, 49–70, doi:10.1080/027868200410840, 2000.

Jimenez, J. L., Canagaratna, M. R., Donahue, N. M., Prevot, A. S. H., Zhang, Q., Kroll, J. H., DeCarlo, P. F., Allan, J. D., Coe, H., Ng, N. L., Aiken, A. C., Docherty, K. S., Ulbrich, I. M., Grieshop, A. P., Robinson, A. L., Duplissy, J., Smith, J. D., Wilson, K. R., Lanz, V. A., Hueglin, C., Sun, Y. L., Tian, J., Laaksonen, A., Raatikainen, T., Rautiainen, J., Vaattovaara, P., Ehn, M., Kulmala, M., Tomlinson, J. M., Collins, D. R., Cubison, M. J., E., Dunlea, J., Huffman, J. A., Onasch, T. B., Alfarra, M. R., Williams, P. I., Bower, K., Kondo, Y., Schneider, J., Drewnick, F., Borrmann, S., Weimer, S., Demerjian, K., Salcedo, D., Cottrell, L., Griffin, R., Takami, A., Miyoshi, T., Hatakeyama, S., Shimono, A., Sun, J. Y., Zhang, Y. M., Dzepina, K., Kimmel, J. R., Sueper, D., Jayne, J. T., Herndon, S. C., Trimborn, A. M., Williams, L. R., Wood, E. C., Middlebrook, A. M., Kolb, C. E., Baltensperger, U., and Worsnop, D. R.: Evolution of Organic Aerosols in the Atmosphere, Science, 326, 1525–1529, doi:10.1126/science.1180353, 2009.

Kautzman, K. E., Surratt, J. D., Chan, M. N., Chan, A. W. H., Hersey, S. P., Chhabra, P. S., Dalleska, N. F., Wennberg, P. O., Flagan, R. C., and Seinfeld, J. H.: Chemical Composition of Gas- and Aerosol-Phase Products from the Photooxidation of Naphthalene, J. Phys. Chem. A, 114, 913–934, doi:10.1021/jp908530s, 2009.

Kessler, S. H., Smith, J. D., Che, D. L., Worsnop, D. R., Wilson, K. R., and Kroll, J. H.: Chemical sinks of organic aerosol: kinetics and products of the heterogeneous oxidation of erythritol and levoglucosan, Environ. Sci. Technol., 44, 7005–7010, doi:10.1021/es101465m, 2010.

Keywood, M. D., Kroll, J. H., Varutbangkul, V., Bahreini, R., Flagan, R. C., and Seinfeld, J. H.: Secondary organic aerosol formation from cyclohexene ozonolysis: Effect of OH scavenger and the role of radical chemistry, Environ. Sci. Technol., 38, 3343–3350, doi:10.1021/Es049725j, 2004.

Kleindienst, T. E., Conver, T. S., McIver, C. D., and Edney, E. O.: Determination of secondary organic aerosol products from the photooxidation of toluene and their implication in ambient $PM_{2.5}$, J. Atmos. Chem., 47, 79–100, doi:10.1023/B:JOCH.0000012305.94498.28, 2004.

Kroll, J. H. and Seinfeld, J. H.: Chemistry of secondary or-

ganic aerosol: Formation and evolution of low-volatility organics in the atmosphere, Atmos. Environ., 42, 3593–3624, doi:10.1016/j.atmosenv.2008.01.003, 2008.

Kroll, J. H., Ng, N. L., Murphy, S. M., Flagan, R. C., and Seinfeld, J. H.: Secondary organic aerosol formation from isoprene photooxidation, Environ. Sci. Technol., 40, 1869–1877, doi:10.1021/Es0524301, 2006.

Kroll, J. H., Donahue, N. M., Jimenez, J. L., Kessler, S. H., Canagaratna, M. R., Wilson, K. R., Altieri, K. E., Mazzoleni, L. R., Wozniak, A. S., Bluhm, H., Mysak, E. R., Smith, J. D., Kolb, C. E., and Worsnop, D. R.: Carbon oxidation state as a metric for describing the chemistry of atmospheric organic aerosol, Nat. Chem., 3, 133–139, doi:10.1038/Nchem.948, 2011.

Kua, J., Hanley, S. W., and De Haan, D. O.: Thermodynamics and kinetics of glyoxal dimer formation: A computational study, J. Phys. Chem. A, 112, 66–72, doi:10.1021/Jp076573g, 2008.

Lambe, A. T., Onasch, T. B., Massoli, P., Croasdale, D. R., Wright, J. P., Ahern, A. T., Williams, L. R., Worsnop, D. R., Brune, W. H., and Davidovits, P.: Laboratory studies of the chemical composition and cloud condensation nuclei (CCN) activity of secondary organic aerosol (SOA) and oxidized primary organic aerosol (OPOA), Atmos. Chem. Phys. Discuss., 11, 13617–13653, doi:10.5194/acpd-11-13617-2011, 2011.

Lanz, V. A., Alfarra, M. R., Baltensperger, U., Buchmann, B., Hueglin, C., and Prevot, A. S. H.: Source apportionment of submicron organic aerosols at an urban site by factor analytical modelling of aerosol mass spectra, Atmos. Chem. Phys., 7, 1503–1522, doi:10.5194/acp-7-1503-2007, 2007.

Lee, A. K. Y., Herckes, P., Leaitch, W. R., Macdonald, A. M., and Abbatt, J. P. D.: Aqueous OH oxidation of ambient organic aerosol and cloud water organics: formation of highly oxidized products, Geophys. Res. Lett., 38, L11805, doi:10.1029/2011GL047439, 2011.

Lim, Y. B., Tan, Y., Perri, M. J., Seitzinger, S. P., and Turpin, B. J.: Aqueous chemistry and its role in secondary organic aerosol (SOA) formation, Atmos. Chem. Phys., 10, 10521–10539, doi:10.5194/acp-10-10521-2010, 2010.

Loeffler, K. W., Koehler, C. A., Paul, N. M., and De Haan, D. O.: Oligomer formation in evaporating aqueous glyoxal and methyl glyoxal solutions, Environ. Sci. Technol., 40, 6318–6323, doi:10.1021/Es060810w, 2006.

Müller, L., Reinnig, M.-C., Warnke, J., and Hoffmann, T.: Unambiguous identification of esters as oligomers in secondary organic aerosol formed from cyclohexene and cyclohexene/α-pinene ozonolysis, Atmos. Chem. Phys., 8, 1423–1433, doi:10.5194/acp-8-1423-2008, 2008.

Ng, N. L., Kroll, J. H., Chan, A. W. H., Chhabra, P. S., Flagan, R. C., and Seinfeld, J. H.: Secondary organic aerosol formation from m-xylene, toluene, and benzene, Atmos. Chem. Phys., 7, 3909–3922, doi:10.5194/acp-7-3909-2007, 2007.

Ng, N. L., Canagaratna, M. R., Zhang, Q., Jimenez, J. L., Tian, J., Ulbrich, I. M., Kroll, J. H., Docherty, K. S., Chhabra, P. S., Bahreini, R., Murphy, S. M., Seinfeld, J. H., Hildebrandt, L., Donahue, N. M., DeCarlo, P. F., Lanz, V. A., Prevot, A. S. H., Dinar, E., Rudich, Y., and Worsnop, D. R.: Organic aerosol components observed in Northern Hemispheric datasets from Aerosol Mass Spectrometry, Atmos. Chem. Phys., 10, 4625–4641, doi:10.5194/acp-10-4625-2010, 2010.

Ng, N. L., Canagaratna, M. R., Jimenez, J. L., Chhabra, P. S., Seinfeld, J. H., and Worsnop, D. R.: Changes in organic aerosol composition with aging inferred from aerosol mass spectra, Atmos. Chem. Phys., 11, 6465–6474, doi:10.5194/acp-11-6465-2011, 2011.

Reinhardt, A., Emmenegger, C., Gerrits, B., Panse, C., Dommen, J., Baltensperger, U., Zenobi, R., and Kalberer, M.: Ultrahigh mass resolution and accurate mass measurements as a tool to characterize oligomers in secondary organic aerosols, Anal. Chem., 79, 4074–4082, doi:10.1021/Ac062425v, 2007.

Robinson, A. L., Donahue, N. M., Shrivastava, M. K., Weitkamp, E. A., Sage, A. M., Grieshop, A. P., Lane, T. E., Pierce, J. R., and Pandis, S. N.: Rethinking organic aerosols: Semivolatile emissions and photochemical aging, Science, 315, 1259–1262, doi:10.1126/science.1133061, 2007.

Rollins, A. W., Fry, J. L., Hunter, J. F., Kroll, J. H., Worsnop, D. R., Singaram, S. W., and Cohen, R. C.: Elemental analysis of aerosol organic nitrates with electron ionization high-resolution mass spectrometry, Atmos. Meas. Tech., 3, 301–310, doi:10.5194/amt-3-301-2010, 2010.

Rudich, Y., Donahue, N. M., and Mentel, T. F.: Aging of organic aerosol: bridging the gap between laboratory and field studies, Annu. Rev. Phys. Chem., 58, 321–352, doi:10.1146/annurev.physchem.58.032806.104432, 2007.

Russell, L. M.: Aerosol organic-mass-to-organic-carbon ratio measurements, Environ. Sci. Technol., 37, 2982–2987, doi:10.1021/Es026123w, 2003.

Russell, L. M., Takahama, S., Liu, S., Hawkins, L. N., Covert, D. S., Quinn, P. K., and Bates, T. S.: Oxygenated fraction and mass of organic aerosol from direct emission and atmospheric processing measured on the *R/V* Ronald Brown during TEX-AQS/GoMACCS 2006, J. Geophys. Res.-Atmos., 114, D00F05, doi:10.1029/2008jd011275, 2009.

Sato, K., Hatakeyama, S., and Imamura, T.: Secondary organic aerosol formation during the photooxidation of toluene: NO_x dependence of chemical composition, J. Phys. Chem. A, 111, 9796–9808, doi:10.1021/Jp071419f, 2007.

Shilling, J. E., Chen, Q., King, S. M., Rosenoern, T., Kroll, J. H., Worsnop, D. R., DeCarlo, P. F., Aiken, A. C., Sueper, D., Jimenez, J. L., and Martin, S. T.: Loading-dependent elemental composition of alpha-pinene SOA particles, Atmos. Chem. Phys., 9, 771–782, doi:10.5194/acp-9-771-2009, 2009.

Sun, Y. L., Zhang, Q., Anastasio, C., and Sun, J.: Insights into secondary organic aerosol formed via aqueous-phase reactions of phenolic compounds based on high resolution mass spectrometry, Atmos. Chem. Phys., 10, 4809–4822, doi:10.5194/acp-10-4809-2010, 2010.

Surratt, J. D., Murphy, S. M., Kroll, J. H., Ng, N. L., Hildebrandt, L., Sorooshian, A., Szmigielski, R., Vermeylen, R., Maenhaut, W., Claeys, M., Flagan, R. C., and Seinfeld, J. H.: Chemical composition of secondary organic aerosol formed from the photooxidation of isoprene, J. Phys. Chem. A, 110, 9665–9690, doi:10.1021/Jp061734m, 2006.

Surratt, J. D., Lewandowski, M., Offenberg, J. H., Jaoui, M., Kleindienst, T. E., Edney, E. O., and Seinfeld, J. H.: Effect of acidity on secondary organic aerosol formation from isoprene, Environ. Sci. Technol., 41, 5363–5369, doi:10.1021/Es0704176, 2007.

Surratt, J. D., Chan, A. W. H., Eddingsaas, N. C., Chan, M. N., Loza, C. L., Kwan, A. J., Hersey, S. P., Flagan, R. C., Wennberg, P. O., and Seinfeld, J. H.: Reactive in-

termediates revealed in secondary organic aerosol formation from isoprene, P. Natl. Acad. Sci. USA, 107, 6640–6645, doi:10.1073/pnas.0911114107, 2010.

Szmigielski, R., Surratt, J. D., Vermeylen, R., Szmigielska, K., Kroll, J. H., Ng, N. L., Murphy, S. M., Sorooshian, A., Seinfeld, J. H., and Claeys, M.: Characterization of 2-methylglyceric acid oligomers in secondary organic aerosol formed from the photooxidation of isoprene using trimethylsilylation and gas chromatography/ion trap mass spectrometry, J. Mass Spectrom., 42, 101–116, doi:10.1002/Jms.1146, 2007.

Takegawa, N., Miyakawa, T., Kawamura, K., and Kondo, Y.: Contribution of selected dicarboxylic and omega-oxocarboxylic acids in ambient aerosol to the *m/z* 44 signal of an aerodyne aerosol mass spectrometer, Aerosol Sci. Technol., 41, 418–437, doi:10.1080/02786820701203215, 2007.

Tolocka, M. P., Heaton, K. J., Dreyfus, M. A., Wang, S. Y., Zordan, C. A., Saul, T. D., and Johnston, M. V.: Chemistry of particle inception and growth during alpha-pinene ozonolysis, Environ. Sci. Technol., 40, 1843–1848, doi:10.1021/Es051926f, 2006.

Ulbrich, I. M., Canagaratna, M. R., Zhang, Q., Worsnop, D. R., and Jimenez, J. L.: Interpretation of organic components from Positive Matrix Factorization of aerosol mass spectrometric data, Atmos. Chem. Phys., 9, 2891–2918, doi:10.5194/acp-9-2891-2009, 2009.

Walser, M. L., Desyaterik, Y., Laskin, J., Laskin, A., and Nizkorodov, S. A.: High-resolution mass spectrometric analysis of secondary organic aerosol produced by ozonation of limonene, Phys. Chem. Chem. Phys., 10, 1009–1022, doi:10.1039/B712620d, 2008.

Wang, W., Kourtchev, I., Graham, B., Cafmeyer, J., Maenhaut, W., and Claeys, M.: Characterization of oxygenated derivatives of isoprene related to 2-methyltetrols in Amazonian aerosols using trimethylsilylation and gas chromatography/ion trap mass spectrometry, Rapid Commun. Mass Spectrom., 19, 1343–1351, doi:10.1002/Rcm.1940, 2005.

Yu, J. Z., Cocker, D. R., Griffin, R. J., Flagan, R. C., and Seinfeld, J. H.: Gas-phase ozone oxidation of monoterpenes: Gaseous and particulate products, J. Atmos. Chem., 34, 207–258, doi:10.1023/A:1006254930583, 1999.

Zhang, Q., Alfarra, M. R., Worsnop, D. R., Allan, J. D., Coe, H., Canagaratna, M. R., and Jimenez, J. L.: Deconvolution and quantification of hydrocarbon-like and oxygenated organic aerosols based on aerosol mass spectrometry, Environ. Sci. Technol., 39, 4938–4952, doi:10.1021/Es048568l, 2005.

Zhang, Q., Jimenez, J. L., Canagaratna, M. R., Allan, J. D., Coe, H., Ulbrich, I., Alfarra, M. R., Takami, A., Middlebrook, A. M., Sun, Y. L., Dzepina, K., Dunlea, E., Docherty, K., DeCarlo, P. F., Salcedo, D., Onasch, T., Jayne, J. T., Miyoshi, T., Shimono, A., Hatakeyama, S., Takegawa, N., Kondo, Y., Schneider, J., Drewnick, F., Borrmann, S., Weimer, S., Demerjian, K., Williams, P., Bower, K., Bahreini, R., Cottrell, L., Griffin, R. J., Rautiainen, J., Sun, J. Y., Zhang, Y. M., and Worsnop, D. R.: Ubiquity and dominance of oxygenated species in organic aerosols in anthropogenically-influenced Northern Hemisphere midlatitudes, Geophys. Res. Lett., 34, L13801, doi:10.1029/2007gl029979, 2007.